
PERGAMON

Journal of the Mechanics and Physics of Solids
48 (2000) 1633–1681

JOURNAL OF THE
MECHANICS AND
PHYSICS OF SOLIDS

www.elsevier.com/locate/jmps

The tribology of rosin

J.H. Smith[a], J. Woodhouse[b,*]

[a]*Bellford Consultancy Services Ltd, 63 Quilter Street, London, E2 7BS, UK*
[b]*Cambridge University Engineering Department, Trumpington Street, Cambridge, CB2 1PZ, UK*

Received 25 May 1999; received in revised form 14 September 1999

Abstract

Rosin is well known for its ability to excite stick–slip vibration on a violin string but the precise characteristics of the material which enable it to exhibit this behaviour have not been studied in any detail. A method is described in which the coefficient of friction of rosin is measured during individual cycles of a stick–slip vibration. Friction versus sliding velocity characteristics deduced in this way exhibit hysteresis, similar to that found in other investigations using different materials. No part of the hysteresis loops follow the friction/velocity curve found from steady-sliding experiments. Possible constitutive laws are examined to describe this frictional behaviour. It is suggested by a variety of evidence that contact temperature plays an important role. Friction laws are developed by considering that the friction arises primarily from the shear of a softened or molten layer of rosin, with a temperature-dependent viscosity or shear strength. The temperature of the rosin layer is calculated by modelling the heat flow around the sliding contact. The temperature-based models are shown to reproduce some features of the measurements which are not captured in the traditional model, in which friction depends only on sliding speed. A model based on viscous behaviour of a thin melted layer of rosin gives predictions at variance with observations. However, a model based on plastic yielding at the surface of the rosin gives good agreement with these observations.

Keywords: Thermomechanical processes; Vibrations; Friction; Constitutive behaviour; Contact mechanics

* Corresponding author: Fax: +44-1223-332662.
E-mail address: jw12@eng.cam.ac.uk (J. Woodhouse).

0022-5096/00/$ - see front matter
PII: S0022-5096(99)00067-8

1. Introduction

In most contexts where stick–slip vibration can occur, it is an undesired effect. For example, in machining it is likely to impair the surface finish of the cut, and in braking systems it may increase wear while reducing braking efficiency. However, there are occasions when stick–slip vibration is deliberately sought, the excitation of violin strings by bowing being the most familiar example. In these latter cases, it is usual to coat the sliding surfaces with rosin (a solid resinous substance obtained by distillation or solvent extraction from various species of coniferous trees, also known as colophony). The frictional properties of rosin make stick–slip vibration much easier to achieve. To understand the detailed physics of such vibration, it is obviously necessary to characterise the tribological behaviour of rosin which gives it this useful effect.

All theoretical work up to now on the bowed string has assumed a very simple model for rosin tribology, in which the coefficient of friction depends only on the instantaneous relative sliding speed between the two contacting surfaces, according to a relationship like that sketched in Fig. 1. The vertical portion of the curve shows the indeterminacy of friction force during sticking, provided the limiting value of friction force is not exceeded. When there is relative sliding, the coefficient of friction drops with increasing sliding speed to a value very

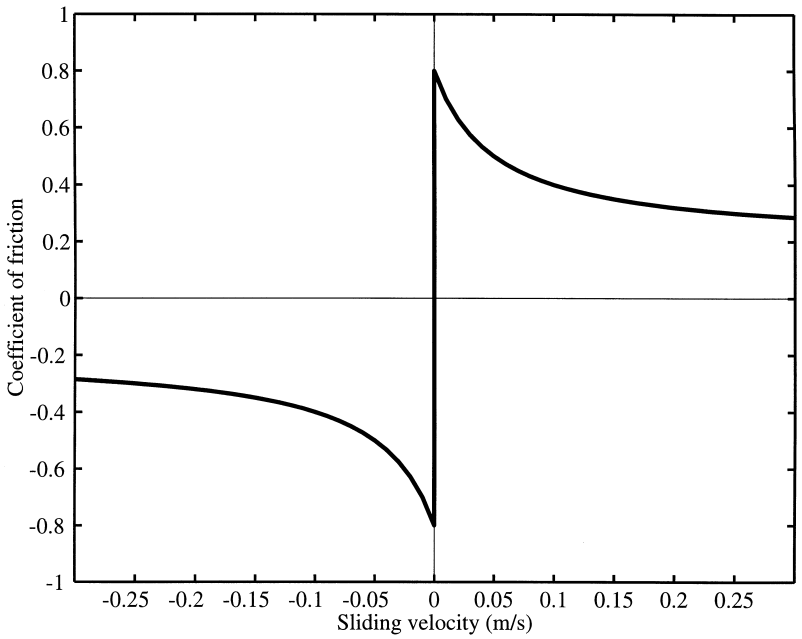

Fig. 1. Sketch of a typical relationship between the coefficient of friction of rosin and instantaneous sliding speed, as assumed in earlier work.

significantly lower than the limit of sticking friction. A number of features of bowed-string motion can be successfully explained in terms of this friction model (McIntyre et al., 1983; Woodhouse, 1993; Schumacher and Woodhouse, 1995; Pitteroff and Woodhouse, 1998), but as investigations probe in more detail it is becoming important to know whether some anomalies arise from shortcomings in this model, and whether the real behaviour of rosin requires a model which is significantly more complicated.

In fact, there appears to be no good physical reason to expect relative sliding velocity to be the only state variable which influences the coefficient of friction. Other aspects of the motion and its history seem likely to play a role. Rosin is a brittle solid at normal room temperatures, but it softens at temperatures only slightly higher. One can imagine that viscosity (or more general visco-elasticity), adhesion, and brittle or ductile fracture might all play some part in the micro-mechanics of stick–slip processes. These in turn might be influenced by, for example, the distance of sliding (perhaps relative to the contact size or to a necking length-scale), or the thermal history around the contact zone.

An obvious approach to such questions is to measure the frictional behaviour directly, during stick–slip vibration with contact conditions not too different from those pertaining to the bowed string problem. An attempt to make such measurements is described in this paper. These show that the usual model for the frictional behaviour of rosin, in which the coefficient of friction depends only on the instantaneous sliding speed, is not correct. The rapid changes in sliding speed encountered in a stick–slip vibration lead to a hysteresis loop in the measured friction/velocity characteristic, and no part of that loop follows the friction/velocity relation deduced from steady-sliding tests. The remainder of this paper is concerned with the search for an alternative constitutive law consistent with these measurements.

Similar questions have arisen in connection with frictional behaviour at other interfaces. For the case of a thin layer of lubricant between, for example, gear teeth, considerable effort has been devoted to characterising lubricant behaviour as a function of contact pressure and temperature. At low pressures lubricants behave as fluids, but if the contact pressure is sufficiently high the behaviour is more like that of a solid, so-called elasto-hydrodynamic lubrication (Johnson, 1985). Other engineering applications are as diverse as the study of asphalt, which has thin layers of bitumen between solid particles, and the stick–slip behaviour of geological faults, related to earthquake modelling. In this latter case, Ruina (1983) has developed a quasi-empirical constitutive model which can reproduce phenomena observed in laboratory experiments using sliding rock surfaces. We take a somewhat similar approach here to the frictional modelling of rosin, but the models to be presented have a more obvious basis in the physics of the underlying behaviour.

Since rosin softens at temperatures not far above normal ambient temperatures, it seems immediately plausible that frictional heating during sliding will influence the tribology. If sufficiently high temperatures were generated, enough to cause substantial softening or melting of the surface layer, the shear strength of the

frictional contact would be weakened considerably and there would be a marked drop in the coefficient of friction. The friction of skates on ice is a familiar situation where this occurs (Bowden and Hughes, 1939). Evidence will be presented that something like this occurs with rosin, and simple models of rosin friction are developed on this basis. The predictions of these models will be compared with the various measurements, and reasonably satisfactory agreement will be demonstrated.

2. Experimental method

2.1. Design of the experimental rig

Dynamic friction force as such is not easy to measure directly under the required conditions. An approach which may be adopted instead is to excite stick–slip oscillation in a system which is well understood, so that one may infer the waveform of force from observations of the motion. The most obvious system for this purpose would be a damped harmonic oscillator. For such a system, sketched in idealised form in Fig. 2, the equation of motion is

$$m\ddot{x} + R\dot{x} + Sx = f(t) \tag{1}$$

so that if the displacement, velocity and acceleration can be determined, the force can be calculated by simple substitution (provided the system mass, stiffness and damping coefficient are known). This method has been applied in previous investigations of friction (Ko and Brockley, 1970), but not to rosin, and with contact conditions which are very far from those applicable to a bowed string. (A preliminary effort has been reported by Schumacher (1997) to make such measurements using an actual bowed string. The results are broadly in line with those to be reported here, and more may be expected of these measurements when further refined.)

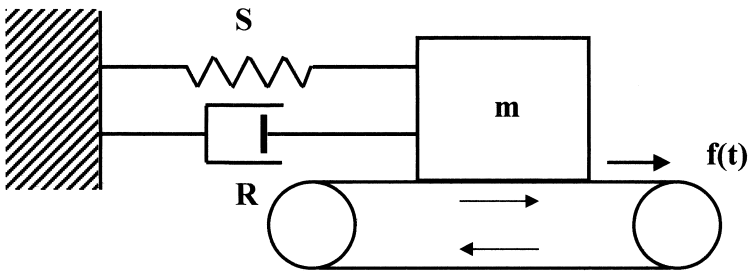

Fig. 2. Frictional excitation of an idealised damped harmonic oscillator.

The conditions we would like to achieve are as follows: the contact geometry between a string and a single hair from a bow is approximately that of crossed cylinders. Normal force varies over quite a wide range, but ordinary steady playing typically involves normal forces of 0.1–10 N (Askenfelt, 1989). This is distributed between the various bow hairs in contact with the string, in a manner which is hard to quantify with any accuracy (Pitteroff and Woodhouse, 1998). Frequencies of oscillation cover most of the audio range: the lowest note of a cello is 65 Hz, the range of notes in first position on a violin is about 200 Hz to 1 kHz, and the highest note on the fingerboard of a violin is around 4 kHz. The motion of a bowed string is such that most of each cycle is spent sticking to the bow, with a speed typically in the range 0.1–1 m/s or so. Sliding is confined to a very short interval, so that sliding speeds can be quite high, up to 10 m/s or so.

This combination of requirements is extremely difficult to match with a laboratory rig which approximates to a harmonic oscillator. The first problem arises from the nature of stick–slip vibration of a harmonic oscillator, compared to that of a bowed string. The "Helmholtz motion" of a bowed string is almost a free motion of the system, sustained by a relatively small fluctuating force from the bow (McIntyre et al., 1983; Schumacher and Woodhouse, 1995). Even though the bow and string are sticking for most of the time during a cycle, a large normal force is not required between them. For a harmonic oscillator, by contrast, the equivalent regime of a nearly-free motion sustained by small input from the bow has only a very short sticking phase during each cycle, and the maximum slipping speed is approximately the same as the bow speed. To achieve a longer sticking phase, and thus a peak slipping speed which is many times the bow speed as in a bowed string, one requires a large normal force. So there is an inevitable conflict between the requirements to match slipping speed and normal force in the contact region.

There are other difficulties in designing a suitable vibrating system for this measurement. The mechanical impedance of a string is rather low, and most other mechanical oscillators present a higher impedance to the bow, again influencing the contact conditions. Efforts to keep the impedance low require that the structure is rather flimsy, which can give rise to problems of stability under the normal load, and also to difficulties with the higher modes of vibration. The nature of the typical waveform of self-sustained frictional oscillation of a harmonic oscillator is such that its Fourier series has some energy in harmonics well above the fundamental. Higher modes of the structure may thus be excited to significant levels, which makes the processing and interpretation of the results more difficult.

The chosen design employed a cantilever arrangement, with a lumped mass on the end of a thin strip. It was machined from Nylon 66 as a single entity, as shown in Fig. 3. This geometry ensures that the mechanical damping (with the cantilever firmly clamped) arises only from linear visco-elasticity in the nylon, not from any micro-slipping which might occur at sharp corners where separate components join. Nylon 66 was chosen for its convenient machining properties and relatively low density, providing a low impedance to vibration and relatively

high damping. The contact region for frictional excitation was generally of a different material — a small wedge of the desired material was glued in place for this purpose.

The cantilever was designed in such a way as to minimise the amplitudes of vibrations other than the fundamental bending mode, so that Eq. (1) provides a good approximation to the true equation of motion. The frequency separation between the first and second bending modes was maximised. Also, to suppress both the second bending mode and the first torsional mode, the excitation point was placed at the intersection of node lines of these modes (in a hole drilled through the cantilever). The measured frequencies of the first two bending modes were 108 and 1625 Hz, and that of the first torsional mode was 602 Hz. The damping of the two bending modes was such as to produce Q factors of 20 for both.

To excite the cantilever into stick–slip vibration, it was "bowed" with a cylindrical rod coated with rosin. This was loaded against the cantilever by an arrangement of wires and weights, as shown in Fig. 3. The rod was attached to a large mass (approximately 16 kg) which could slide on an air bearing. This was driven by hand, producing a sufficiently steady velocity which was monitored by a displacement transducer. Vibration of the cantilever was observed using a small accelerometer placed as close as possible to the driving point. The accelerometer signal was captured in digital form by a data-logger running at 50 kHz, subsequent processing being carried out by computer. Data capture was initiated at a pre-determined position, so that measurements could be repeated with the same section of the rod surface in contact. Before each measurement, the normal load at the contact was checked with the rod in the relevant position, by measuring the minimum force required to separate the contacting surfaces. The necessary vibration data, covering a few stick–slip cycles, was collected over only a few millimetres of travel, so that both the normal load and the velocity of the

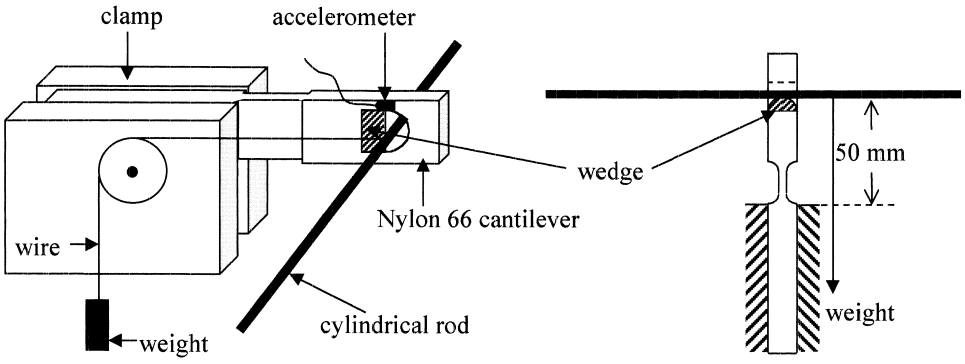

Fig. 3. Schematic diagram of the experimental rig. The cross-section is shown correctly to scale.

rod could reasonably be assumed constant over the measurement period (typically 0.2 s).

2.2. Experimental procedure

The result of a given measurement run using this apparatus was a sampled waveform of acceleration covering several stick–slip cycles. To deduce the contact frictional force $f(t)$ from Eq. (1), the velocity and displacement waveforms were also required, so the signal was integrated numerically. The mean frictional force will produce a non-zero mean value of the displacement waveform, which cannot be deduced from the acceleration, so this was determined from the output of separate (non-contacting) displacement transducer. The self-consistency of the two measurements was checked, and any DC offsets in the instrumentation amplifiers determined and corrected, by comparing the twice-integrated acceleration signal with the measured displacement signal. A least-squares fitting procedure was used to calculate the offsets and obtain the best match between these two signals. For all the results to be presented here, a very accurate match was obtained.

The force $f(t)$ could then be calculated, once the equivalent mass, stiffness and damping of the first bending mode of the cantilever were known. The stiffness S was deduced from the output of the displacement transducer in response to static loading of the cantilever in this mode. The values of mass m and dashpot rate R then follow from the frequency and Q factor given above. The results were $S = 7.6$ kN/m, $m = 0.017$ kg and $R = 0.56$ Ns/m. Note that the impedance $\sqrt{Sm} = 11$ Ns/m. This compares with a value of the order of 0.2 Ns/m for the wave impedance of a typical violin string (Pickering, 1992; Schumacher, 1994), illustrating the problem of designing a simple oscillator with properties very close to those of a string.

Results have been obtained using a variety of materials for the rod. It is also possible to vary the material of the wedge forming the contact region in the cantilever, but all the results reported here used perspex (polymethyl methacrylate) for this wedge. In order to excite stick–slip vibration, the rod was coated with a film of rosin. This was applied in the same manner that a violinist applies rosin to the hair of a normal bow, by rubbing a block of rosin against the surface. Since rosin softens at temperatures not far above room temperature, the frictional heat generated by the rubbing is sufficient to transfer a layer of rosin to the surface being coated, probably by a process involving partial melting. More will be said about the thermal behaviour of rosin in the Section 4.

To provide a comparison for the dynamic friction measurement obtained by this approach, the steady-sliding characteristics of the same surfaces were also measured. The wedge was removed from the cantilever and clamped rigidly. The rosined rod was loaded against it and driven, in exactly the same manner as described above. In this case the frictional force was measured using a piezoelectric force transducer mounted in the rod. This approach is not sufficiently accurate for the dynamic measurements, since inertial and dissipative effects associated with the rod dynamics will modify the force waveform under stick–slip

conditions. However, for steady-sliding measurements we require only quasi-steady forces, and these effects do not then matter. The rod velocity was measured in this case by attaching a displacement transducer to the air bearing, and determining an average velocity over the measurement period.

3. Experimental results

3.1. Steady sliding

The steady-sliding results are shown in Fig. 4. Each point was determined by sliding a perspex rod coated with rosin at the appropriate constant velocity over a perspex wedge. The results show a very marked decrease in friction coefficient with increasing sliding speed. The results are very similar to those obtained previously by Lazarus (1972) using a similar method. For use in the simulations to be described in Section 5, a curve-fit to the data of Fig. 4 has been made:

$$\mu = 0.4\exp(-V/0.01) + 0.45\exp(-V/0.1) + 0.35 \tag{2}$$

where the sliding speed V is measured in m/s. The solid line in the figure shows this fitted function.

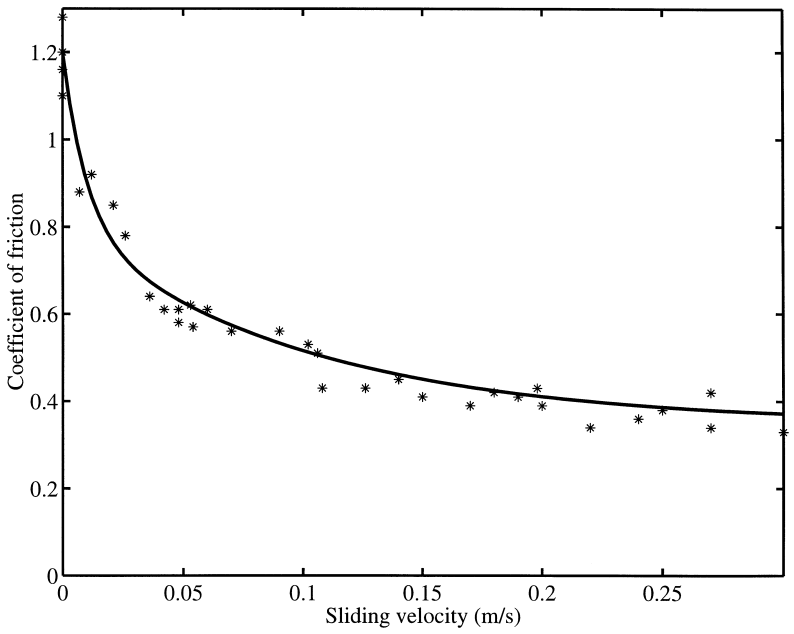

Fig. 4. Measured friction versus sliding speed characteristic of rosin. Each point is measured during steady sliding at constant velocity. The solid line indicates the curve-fit of Eq. (2).

3.2. Sinusoidal forced sliding

A first indication that this steady-sliding characteristic is not appropriate for predicting dynamic friction forces may be obtained by a very simple experiment. Using the same set-up as for the steady sliding tests, the rod was pushed back and forth against the wedge with an approximately sinusoidal waveform at about 4 Hz. At such a low frequency, the signal from the force transducer mirrors the friction force reasonably accurately. The reading is contaminated by inertial effects from the rod, tension effects from the arrangement for the normal load, and excitation of stress waves in the rod. These were all assessed by independent measurements, and it was found that for this low frequency of sinusoidal excitation the net effect was to influence the coefficient of friction by less than ± 0.1.

For one particular case the variation of friction coefficient as a function of time is plotted in Fig. 5(a). Plotting the measured behaviour in the friction/velocity plane yields Fig. 5(b). Fig. 5(c) and (d) show corresponding close-up views of the detailed behaviour near one of the transitions where the friction force and sliding velocity change sign. Corresponding plots to Fig. 5(a) and (b) for a case in which the maximum velocity was significantly higher are shown in Fig. 5(e) and (f). During the intervals of sliding the results are somewhat noisy (due presumably to irregularities in the surfaces and to dynamic effects contaminating the force measurement), but a fairly consistent picture can be seen. The curve fit of Eq. (2) is superimposed on Fig. 5(b), (d) and (f) as a dashed line.

The most striking difference between the dynamic and steady friction characteristics is that there is hysteresis: the results in Fig. 5(b) and (f) trace out a pair of loops, with higher forces immediately after "sticking" (i.e. zero sliding speed) and significantly lower ones when the sliding speed approaches zero again. In other words, the hysteresis loops are traversed in a clockwise direction. The upper part of these hysteresis loops follows the steady-sliding curve fairly closely, but the lower part does not. Near zero sliding speed, the curves have a steep but finite slope rather than the infinite slope of the idealised Fig. 1. This finite slope is not an artefact of the measurement resolution, the sloping portion is well resolved, as is shown in the magnified view of Fig. 5(c) and (d). (The high-frequency oscillation following the positive peak of friction force is a result of compressional waves in the perspex rod excited by the rapid change of friction force.) Another feature visible in the results of Fig. 5 is, however, probably an artefact of the experimental procedure: in both cases, the behaviour of the friction coefficient is slightly asymmetric between positive and negative sliding speed. This apparently arises from asymmetry in the waveform produced by hand-excitation of the air-bearing mass.

3.3. Stick–slip oscillation

A typical set of results from the stick–slip apparatus is shown in Fig. 6. In this case a rosin-coated wooden rod was used, with normal load 6.3 N and rod

velocity 0.042 m/s, against a perspex wedge. The output from the accelerometer (Fig. 6(a)) shows that during the sliding phase of the motion, the waveform is very roughly sinusoidal with a period corresponding to the first mode of vibration of the cantilever. During the sticking phase, the contact point on the cantilever moves at the same velocity as the rod. The abrupt transition to sticking excites the

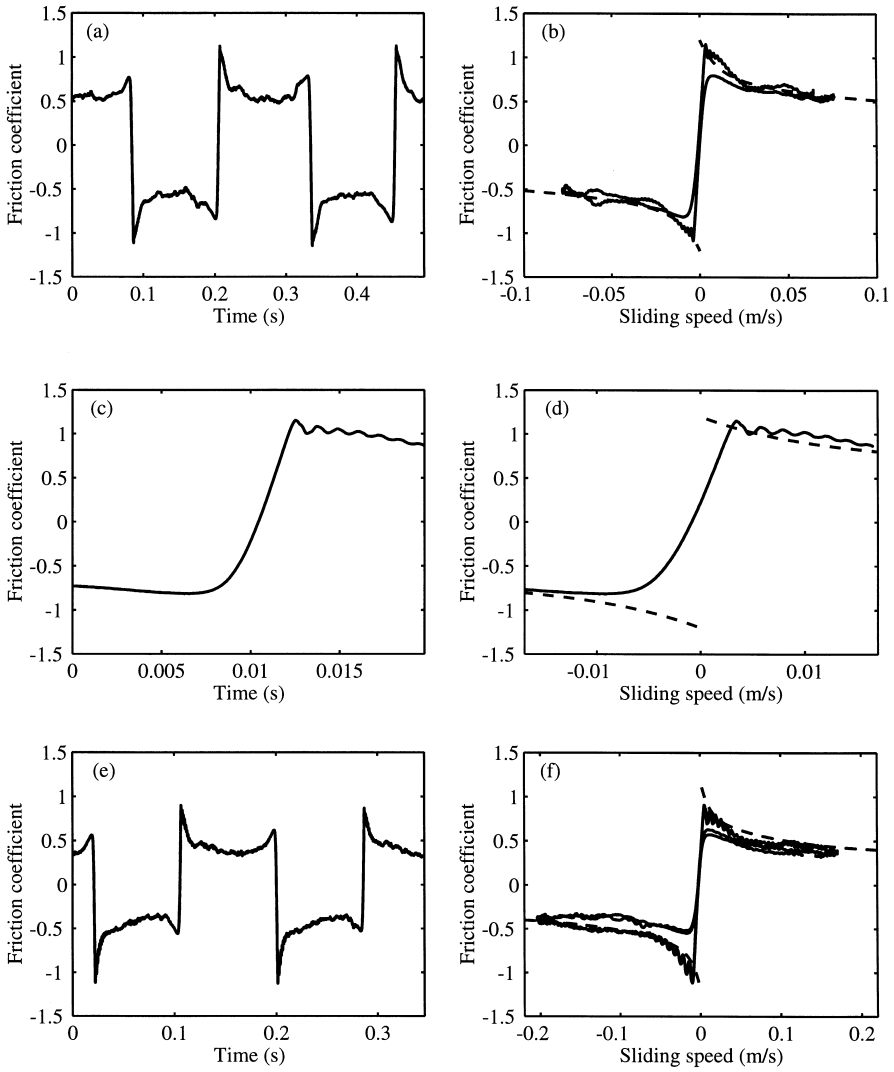

Fig. 5. Friction versus sliding speed characteristic, during forced sinusoidal sliding of a rosin-coated perspex rod on a perspex wedge. The exponential curve fit from Fig. 4 is shown as a dashed line, for comparison. Pictures (c) and (d) show one of the abrupt transitions of (a) and (b), respectively, on a greatly expanded scale. Normal load is 3 N in all cases.

higher frequency modes of the cantilever, visible in the plot because the accelerometer could not be placed exactly at the contact point. The corresponding velocity waveform is shown in Fig. 6(b).

The friction–velocity characteristic calculated from these waveforms is plotted in Fig. 6(c), with the steady-sliding characteristic superimposed as a dashed line. Note that the curve appears horizontally reversed relative to the plots shown in Figs. 1, 4 and 5. This is because the earlier figures had relative sliding speed on the horizontal axis, whereas here we have the speed $v(t)$ of the contact point, in terms of which the sliding speed is $v_b - v$ where v_b is the "bowing" speed. Fig. 6(c) shows an anticlockwise hysteresis loop, the corresponding sense to those seen in Fig. 5: at the end of the sticking phase, the coefficient of friction has reached a maximum static value of approximately 0.85. Once sliding begins the coefficient falls sharply, in a qualitatively similar manner to the steady sliding characteristic. However, a different path is traced out prior to returning to the sticking phase, with only a small increase in the friction coefficient being observed.

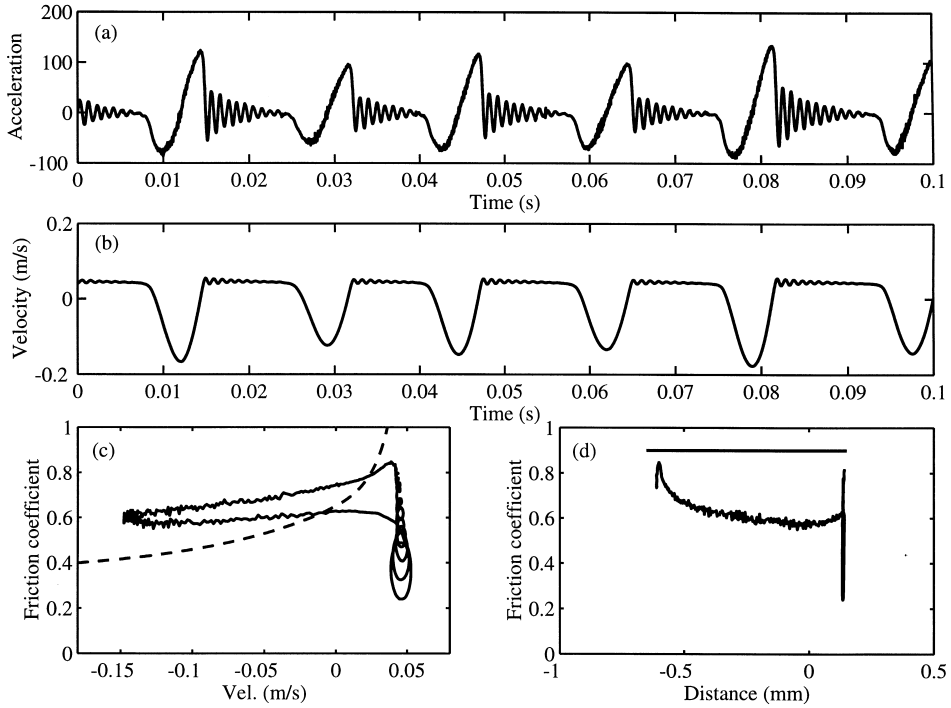

Fig. 6. Typical set of results from the stick–slip apparatus, obtained using a rosin-coated wooden rod, with normal load 6.3 N and rod velocity 0.042 m/s, against a perspex wedge: (a) acceleration/time history; (b) velocity/time history; (c) friction coefficient versus measured velocity (with exponential curve fit from Fig. 4 superimposed as a dashed line); (d) friction coefficient versus sliding displacement (with contact patch diameter shown as a solid line).

During sticking, the plot does not show a single line, but instead has visible loops. This is an artefact of observing the acceleration a small distance away from the contact point: during sticking the cantilever can move in a vibration mode which involves rotation about the contact point, which is picked up by the accelerometer and produces the obvious decaying oscillations seen in Fig. 6(a). This shortcoming in the instrumentation does not degrade the results in any serious way: the decaying oscillation picked up during the sticking phase is symmetrical about the correct sticking velocity, so the right result is obtained by imagining the loops collapsed horizontally to their mean position.

Fig. 6(c) shows very clearly that instantaneous sliding speed does not determine the coefficient of friction during a stick–slip vibration. There is a large hysteresis loop, and (unlike the result of sinusoidal excitation seen in Fig. 5) no part of that loop follows the steady-sliding curve, even approximately. Another simple state variable which might play a role is sliding distance, and in Fig. 6(d) we show how the frictional force varies with sliding distance throughout a stick–slip cycle. The estimated contact patch size is shown to give a relative scale. (The contact patch was examined under an optical microscope to make this estimate.) In this view, the frictional force falls dramatically with increasing distance from the sticking position then retains a fairly constant value throughout the sliding period.

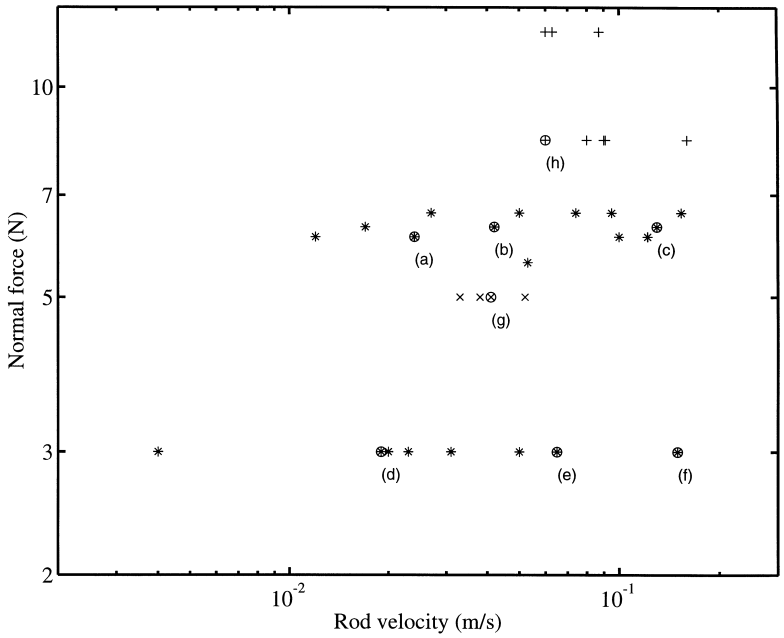

Fig. 7. Summary of the measurements obtained from the stick–slip rig using rosin-coated surfaces over a range of normal force and rod velocity. A perspex wedge was used in all cases. The rod material was wood (∗), perspex (×) or steel (+). Circles indicate cases illustrated later.

Similar stick–slip tests have been carried out over wide ranges of normal force and rod velocity. These are summarised in Fig. 7. A selection of these cases, labelled (a)–(f), will be used to illustrate how the behaviour varies with the rod velocity and normal force. The results in this set were all obtained using a wooden rod sliding against a perspex wedge. Case (b) was the one shown in Fig. 6. Results will also be shown for one case of a perspex rod against a perspex wedge, labelled (g), and one using a steel rod against a perspex wedge, labelled (h).

Fig. 8 shows the effect on the acceleration waveforms of changing rod speed. These are the cases labelled (a)–(c) in Fig. 7, with a normal load of approximately 6 N, but a very similar variation is seen along any horizontal line in Fig. 7. The sticking phase of the cycle tends to reduce as the rod velocity increases, until the motion becomes quasi-harmonic at very high rod speed. The waveform during sliding is rather similar in each case.

The set of friction–velocity characteristics determined from the tests labelled (a)–(f) in Fig. 7 are shown in Fig. 9. The figures are laid out spatially to correspond to the points in Fig. 7, with normal force varying vertically and rod speed horizontally. In each case, the steady sliding characteristic is shown superimposed as a dashed line. The overall impression is that the measured curves

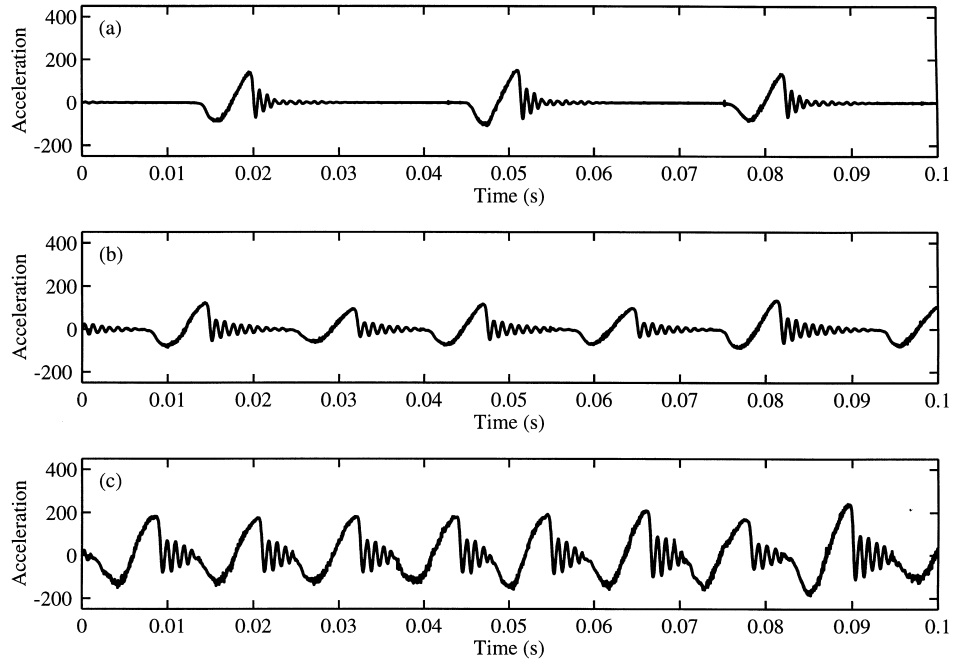

Fig. 8. Acceleration waveforms showing the effect of changing the rod velocity. These waveforms correspond to tests (a), (b) and (c) in Fig. 7, with normal force approximately 6 N, sliding velocity (a) 0.024, (b) 0.042 and (c) 0.13 m/s.

are mostly rather similar in shape. They all have anticlockwise hysteresis loops, and none of them shows any tendency to follow the steady-sliding characteristic. Generally, the maximum coefficient of friction (at the end of sticking) is rather lower than the steady result, while once sliding has begun the coefficient of friction stays higher than the steady results would suggest.

A significant observation about Fig. 9 is the negative one, that no conspicuous variation occurs in the friction/velocity characteristic with either force or rod speed. This will prove to be an important fact when comparisons are made with possible theoretical models. Looking carefully, however, two minor trends are perhaps discernible. First, at low rod speeds the coefficient of friction tends to be higher: this is especially true of the peak value at the end of sticking. Second, the hysteresis loops are somewhat more open at lower speed and force, collapsing to a longer and thinner form at high speed and force.

The friction–velocity characteristic shown in Fig. 10(a) was obtained using a perspex rod rather than a wooden one, under conditions marked at position (g) in Fig. 7. The hysteresis loop (still anticlockwise) has a significantly different form, the falling portion after the peak value being rather straight. This contrasts with the more "peaky" shape obtained with a wooden rod, seen in Fig. 9. Much of the high frequency noise observed in the friction characteristics of Fig. 9 is absent here, perhaps because the rosin has coated the perspex rod with fewer surface irregularities. Several measurements were made on separate occasions using this perspex rod, attempting to reproduce the same sliding conditions as in Fig. 10(a). These showed good agreement in the shape of the hysteresis loop and in the values of static and dynamic friction coefficients, confirming that the measurement

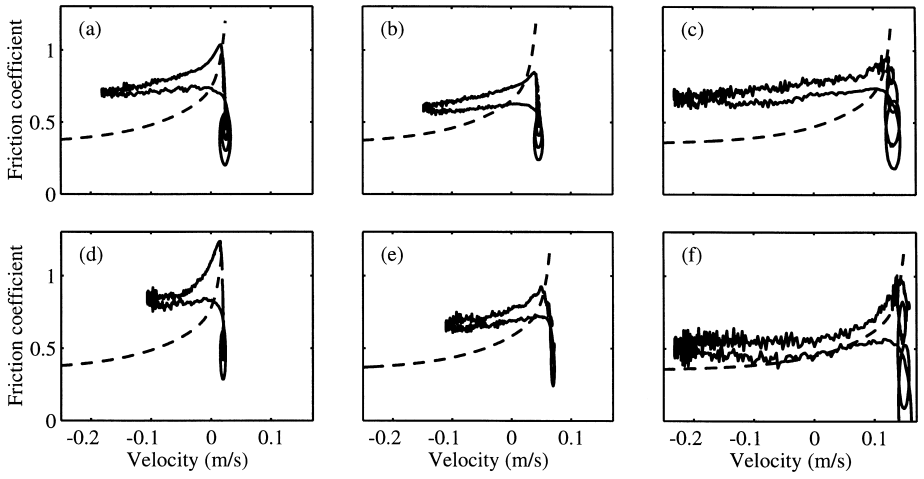

Fig. 9. Friction–velocity characteristics determined from the tests marked (a)–(f) in Fig. 7. The steady sliding characteristic is shown superimposed for comparison.

procedure is capable of good repeatability. Consecutive stick–slip waveforms taken from a single measurement were also found to be repeatable.

Finally, Fig. 10(b) shows a typical friction–velocity characteristic obtained using a steel rod on a perspex wedge, under conditions marked at position (h) in Fig. 7. To coat a metal rod with rosin requires warming the rod first, and the rosin remains attached for only a few passes through the stick–slip contact. However, while the rosin is in place stick–slip motion can be readily excited. The resulting friction–velocity characteristic is not too different from those obtained with the wooden rod, shown in Fig. 9.

3.4. Accuracy checks

It is important to be sure that the observed hysteresis loops and anomalous values of friction coefficient are genuine physical phenomena rather than artefacts of the experimental details. We should note in passing that similar hysteresis has been reported by Ko and Brockley (1970), using lubricants rather than rosin in the contact region.

It has been suggested (Tolstoi, 1967) that frictional hysteresis is caused by variations in the normal load during the stick–slip vibration. For this to be the case in the apparatus used here would require a large variation in the normal load to occur at the stick–slip frequency, since the measured friction varies by up to 40% around the hysteresis loops. In the absence of a contact resonance in this frequency range or other modes of vibration of the apparatus, there is no obvious mechanism by which such large fluctuations in normal force could occur. There is also no obvious mechanism for triggering this vibration, the only likely one being the small normal component of the stick–slip vibration, which results from the cantilever being of finite length so that the point of contact traces an arc. The amplitude of the normal vibration was measured directly using an accelerometer attached to the rod. It was found to be too small to account for the observed

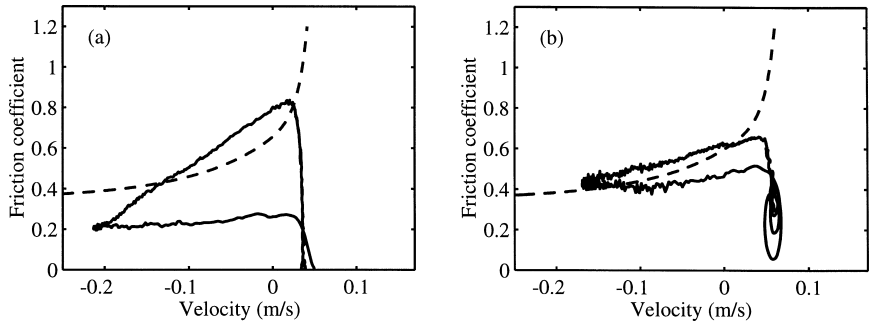

Fig. 10. Friction–velocity characteristics determined from the tests marked (g) and (h) in Fig. 7: (a) test (g), perspex rod, normal force 5 N, speed 0.041 m/s; (b) test (h), steel rod, normal force 8.4 N, speed 0.06 m/s. The steady sliding characteristic is shown superimposed for comparison.

hysteresis: indeed, it was so small that it was difficult to distinguish from noise produced by the much larger lateral and axial vibration via cross-sensitivity of the accelerometer.

Various factors limiting the accuracy of the frictional force waveform derived from Eq. (1) have already been mentioned: the problem of measuring the vibration at the point of contact, the presence of higher modes of vibration, and possible inaccuracies in calibration. These are all associated with the design of the apparatus. The sensitivity of the results to these factors can be explored by processing simulated waveforms as if they were experimental data: it is easy to vary these factors at will in a simulation, and of course the frictional model used in the simulation is known exactly. The method of simulation will be described in detail in Section 6.1.

A series of tests has been made, using simulated stick–slip waveforms based on a theoretical model of vibrational properties of the cantilever, and the traditional frictional model in which the friction force is governed by the sliding speed according to a relation like that shown in Fig. 1. Fig. 11(a) shows the result of reconstituting the friction law using the correct parameters for the cantilever behaviour. As expected, it accurately follows the law assumed in the simulation. An error in the effective mass and stiffness of the oscillator which leaves the resonant frequency unchanged has the result of simply scaling this curve by a constant factor. Fig. 11(b) shows the effect of a 2% error in the fundamental frequency of the cantilever. Here, a small hysteresis loop is created (clockwise when the frequency is too high, anticlockwise when it is too low). This loop does not have the same form as the loops seen in the measurements, and in any case the oscillator frequency is in practice known to within 1% accuracy. The conclusion is that the observed hysteresis is unlikely to be influenced significantly by such errors.

The data processing to produce the friction coefficient could also be a source of inaccuracy. One obvious factor in the accuracy of the calculation is the sampling

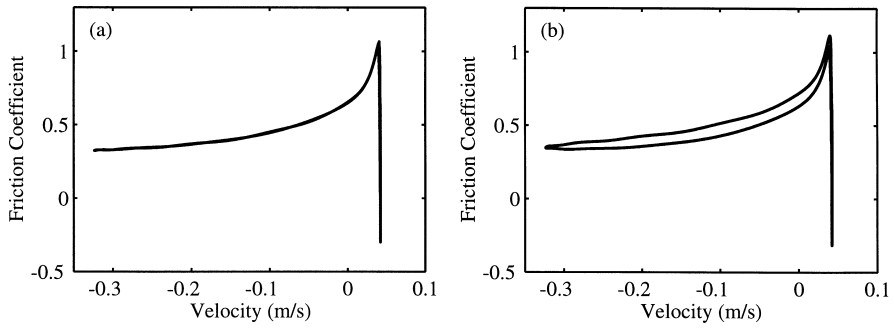

Fig. 11. Assessment of the sensitivity of the data processing method: (a) friction–velocity characteristic processed from simulated data with an assumed friction law using correct parameters for the oscillator; (b) the effect of a 2% error in the fundamental frequency of the oscillator.

frequency of the measurements. This is easily explored by varying the sampling rate. A 25 kHz sampling frequency was found to be sufficient for the calculation to converge, and to provide a margin of safety all the measurements reported here were obtained from data sampled at 50 kHz. The numerical integration necessary to obtain the velocity signal was adequately tested by the fact that, for all cases shown here, the twice-integrated acceleration signal and the measured displacement signal were in excellent agreement over the entire length of the data sample (normally 0.2 s). From all these tests, it may be concluded that the measured curves of Figs. 9 and 10 show real physical effects which are not seriously degraded by experimental artefacts.

4. Thermal model of rosin

4.1. Properties of rosin

At room temperature rosin is an extremely brittle solid which fractures in a glassy manner and powders easily. It is extracted from the resin of various species of coniferous tree. Its chief constituent is abietic acid, and it is soluble in organic solvents. Various grades exist according to the age of the tree from which the resin is drawn and the amount of heat applied in distillation. These range from a rather opaque black substance to a transparent colourless one. The possibility of transparency suggests that the material is amorphous rather than polycrystalline. Some material characteristics of a sample of rosin are summarised in Table 1. The quoted values of thermal conductivity and specific heat capacity are taken from the measurements of Cobbold and Jackson (1992).

Melting was investigated qualitatively by slowly heating a small amount of rosin. By about 60°C it becomes possible to make a visible indent with the point of a knife. Rather than melting at a well-defined temperature the rosin then softened progressively, turning into a thick and sticky liquid by about 75°C. It then gradually became less viscous until it can be poured readily at 93°C.

Quantitative measurements were made in a rheometer (Rheometrics RDS II). A layer of rosin 1.5 mm in thickness was cast while hot between two aluminium discs of 25 mm diameter. This sandwich was mounted in the rheometer, and sinusoidally oscillating shear strain was applied. The complex shear modulus of the rosin layer was determined, over a controlled range of strain and temperature,

Table 1
Material properties used in simulations

	Rosin	Perspex	Wood
Density (kg/m^3)	1010	1200	600
Thermal conductivity (W/m/K)	0.113	0.2	0.2
Specific heat capacity (J/kg/K)	250	1460	1680

and at two different frequencies. Throughout the range studied, the rosin remained firmly stuck to the aluminium discs so that the bulk properties were measured. In all cases, the behaviour was found to be predominantly viscous (the phase angle of the complex modulus being greater than 70°), and essentially independent of strain amplitude provided the amplitude was small enough not to cause additional heating. Strains were small throughout the test, and at the lower temperatures they were extremely small since the material was so fragile. Each measured point was the result of a strain sweep over a range, and points were only accepted if the value was essentially constant during the sweep. This eliminates the danger of additional shear heating in the rosin sample contaminating the results.

The measured viscosity fell by approximately four orders of magnitude in the temperature range 45–85°C, as shown in Fig. 12. There was some variation with excitation frequency: measurements at very low frequency gave consistently higher values of viscosity than measurements at higher frequency. The higher of the two testing frequencies seems more appropriate to the oscillatory phenomena under investigation here, and at this frequency the variation of viscosity with temperature followed an exponential trend, quite well approximated by the function

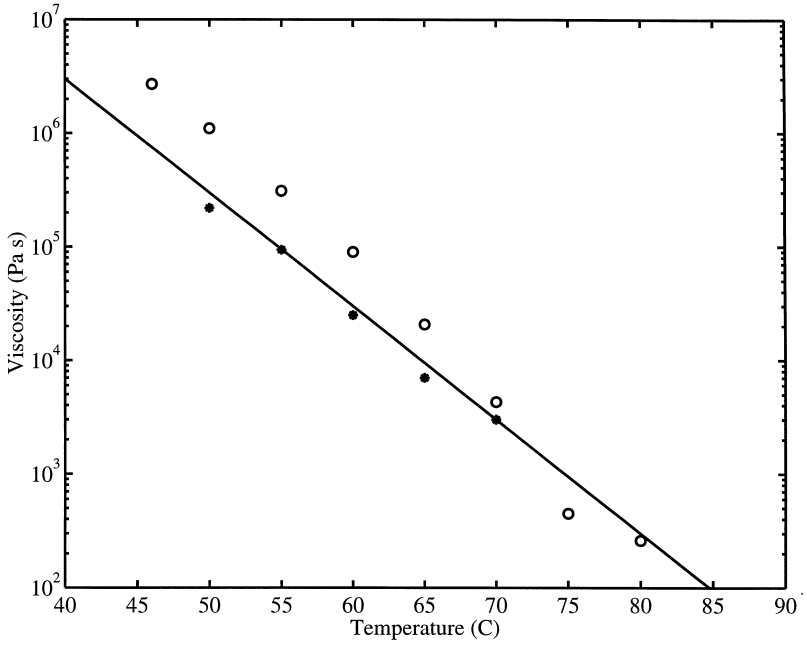

Fig. 12. Measured viscosity of rosin as a function of temperature; open symbols: frequency 1 rad/s, solid symbols: frequency 100 rad/s, solid line: curve fit of Eq. (1).

$$\eta = 3000 \times 10^{\left(\frac{50-T}{10}\right)} \text{ Pa s} \tag{3}$$

where T is the temperature in Kelvin above ambient (taken as 20°C). The law is expressed in this form for compatibility with modelling to be presented shortly, when all temperatures will be measured relative to this ambient level. Very similar results were reported by Cobbold and Jackson (1992), using a different design of apparatus. Exponential variation of viscosity with temperature is essentially the behaviour predicted by the simple Eyring model (Tabor, 1979). (Strictly, this model predicts variation proportional to the exponential of the inverse of the absolute temperature. Since our measurements cover a very restricted range of absolute temperature from 319 to 353 K, a binomial expansion of the inverse temperature is justified, to give the result as measured.) For the lower temperatures in the measured range, even though the bulk rosin in the test behaved as a "viscous liquid", the viscosity is very high. Under the different conditions of interfacial stick–slip motion, it might be expected to behave as a solid except over long (creep) timescales.

4.2. Evidence of thermal softening

Evidence that heating plays some role in the frictional behaviour of rosin may be inferred from the way in which rosin transfers to various materials. When a block of rosin is rubbed against a copper surface, it forms a powder which does not adhere well to the surface, whereas if the copper is warmed above the rosin softening temperature range first, rosin transfers as a semi-molten film which adheres fairly well as it re-solidifies. By contrast, a film of rosin transfers to a rod of perspex (polymethyl methacrylate) or wood very readily. Presumably, the frictional heat generated by the rubbing action is not dissipated so rapidly by conduction, so that it is possible to deposit a film by local melting. Similarly, in the stick–slip apparatus described earlier, when a steel rod coated with rosin was used to excite stick–slip vibrations, the rosin did not hold for long and steady sliding occurred when all the rosin was worn away. A perspex or wooden rod, on the other hand, continued to excite stick–slip after a considerable length of time, perhaps because continued heating during sliding helped the rosin to remain stuck to it.

To investigate further whether melting does indeed occur, the surface of a block of rosin was examined in a scanning electron microscope after cylindrical rods of various materials with widely differing thermal conductivities were rubbed against it. The rosin block was first shaped and polished using a fine grade of emery paper so that it had an approximately cylindrical surface of similar radius to the rods, to give an approximately circular contact patch. The rods were thoroughly cleaned before sliding each of them by hand across the rosin surface for a few centimetres in the same direction, at an estimated velocity of 0.1 m/s and normal load of 5 N. This procedure was carried out in a clean room to prevent the accumulation of dust particles at the contact. The rosin surface was then coated

with a thin layer of gold so that it could be observed in the scanning electron microscope.

Some typical photographs of the wear scars are shown in Fig. 13. The direction of sliding is up the page, and perpendicular to the direction of the initial polishing, the evidence of which can be seen surrounding each wear scar. Fig. 13(a) and (b) show the wear scar produced by a wooden rod. The general view shows a uniform, smooth surface with some streaks in the general direction of sliding. The close-up picture of the top edge of the scar, where the temperature was probably highest, shows rather clear evidence of flow, with traces of the earlier polishing marks showing through where molten material has been dragged across more solid material. Some degree of melting has surely occurred here. By contrast, cracks on the surface generated by a copper rod, shown in Fig. 13(c) and (d), have not been smeared to anything like the same degree, and have a more angular appearance. The rosin may have been softened by the passage of the copper rod, but it does not appear to have melted.

4.3. Review of melt lubrication

Localised melting at a sliding contact causes a marked reduction in the coefficient of friction between two materials. This is caused by melt lubrication, in which sliding is lubricated by a layer of molten material which is produced at the interface by frictional heating (Sternlicht and Apkarian, 1960). For a material with a definite melting temperature an ingeniously simple argument can be used. As material melts, it tends to be squeezed out of the contact and melt wear occurs (Lim and Ashby, 1987). Thus, regardless of the amount of heat available for melting, the film of molten liquid at the contact remains thin. The presence of solid and liquid in close proximity at the contact means that the temperature at the contact must be very close to the melting point of the material.

Evans et al. (1975) used this argument in considering the coefficient of friction of ice. They assume that as soon as sliding begins, the temperature of the contact rises to 0°C and does not rise above it. The amount of heat which is conducted away is therefore restricted and can be calculated as that which is required to maintain the contact at 0°C. The remaining frictional heat melts a layer of ice which lubricates sliding. Evans et al. (1975) proposed that as the sliding speed increases, instead of the amount of heat available for melting increasing, the coefficient of friction falls. If only a small amount of melting occurs, the coefficient of friction can be calculated straightforwardly from the assumption that the coefficient of friction adjusts itself so that just sufficient heat is generated at the contact to keep the contact temperature at the melting point. The dependence of the coefficient of friction both on the sliding speed and on the ambient temperature turns out to be well approximated by this calculation, without any physical basis for the friction mechanism being given.

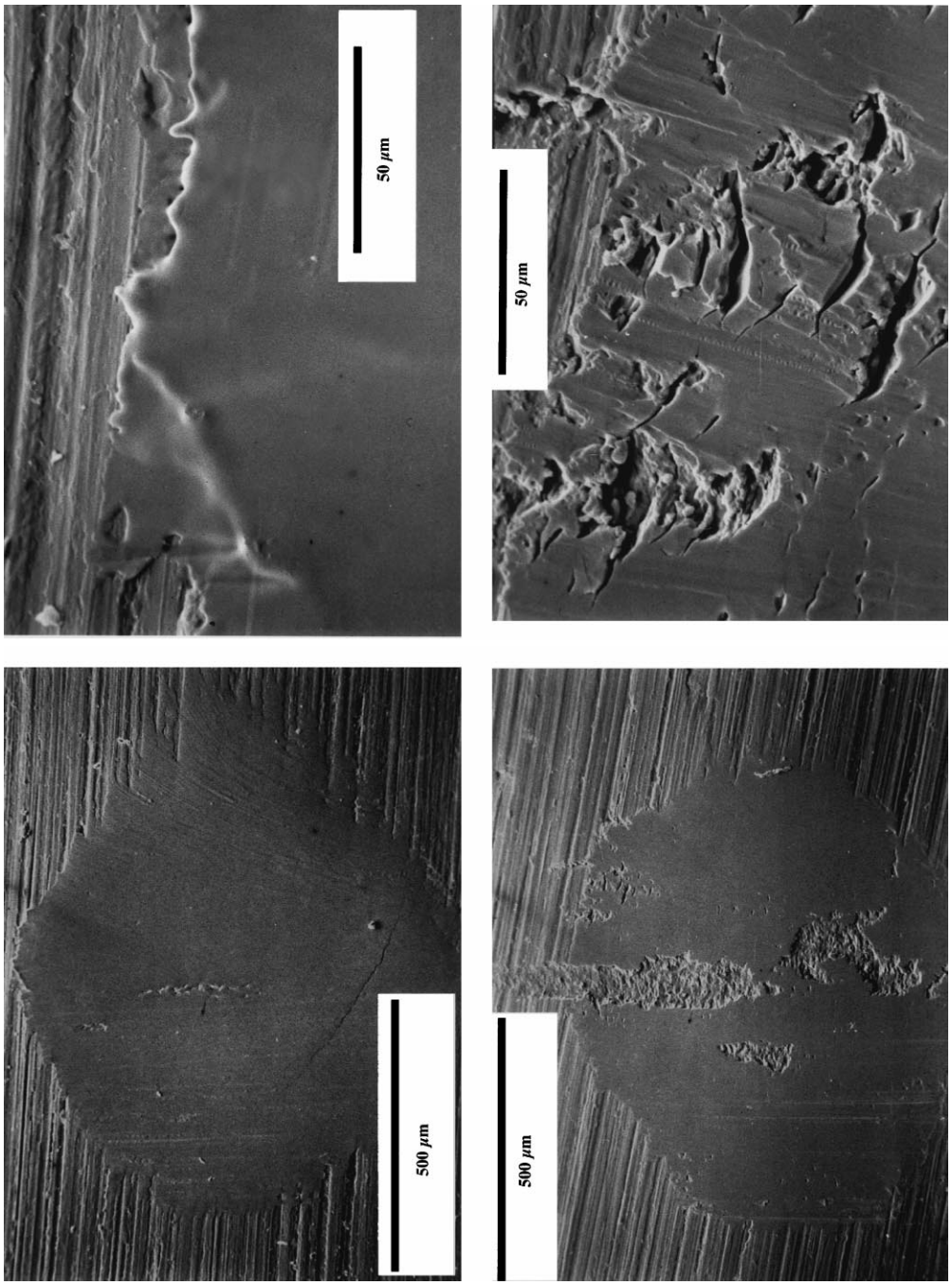

Fig. 13. Wear scars produced by sliding rods of different materials over a rosin surface: (a–b) wooden rod; (c–d) copper rod. Direction of sliding was vertically up each picture.

4.4. Melt lubrication model for rosin

Since the melting, or softening, of rosin occurs over a range of temperature, some form of melt lubrication might be expected well before the rosin becomes fully liquid. The approach used by Evans et al. (1975) cannot be used to deduce the coefficient of friction of a rosin layer, since the temperature at the interface is not fixed at a well-defined melting temperature during sliding and it is therefore not possible to calculate the coefficient of friction directly from the amount of heat conducted away from the contact.

Even for the simple configuration of the rosin experiments reported earlier, the full three-dimensional details of heat and material flow in the contact region are rather complicated. The geometry of the contact is that of two crossed cylinders loaded together to give an approximately circular contact area. The normal force distribution over this region will presumably be approximately that of classical Hertzian contact (Johnson, 1985). One of the cylinders is stationary, while the other moves across it carrying a layer of rosin, as sketched in Fig. 14. This rosin will be at ambient temperature on entry to the contact zone (unless it is still warm from a previous episode in the contact region, a possibility we ignore). It will behave as a solid, and initially will slide over the surface of the fixed cylinder.

As it moves further into the contact zone frictional energy will heat the surface of the rosin layer, perhaps sufficiently that it sticks to the fixed cylinder. There would then perforce be a layer of some thickness within which shearing motion is taking place. This might be a relatively thick layer within which the deformation is best described as viscous flow, or it might be a thin interfacial layer better described by visco-plastic yielding of rosin in a "mushy solid state". Once shearing motion is established in a layer of some thickness, the volume flow rate of rosin

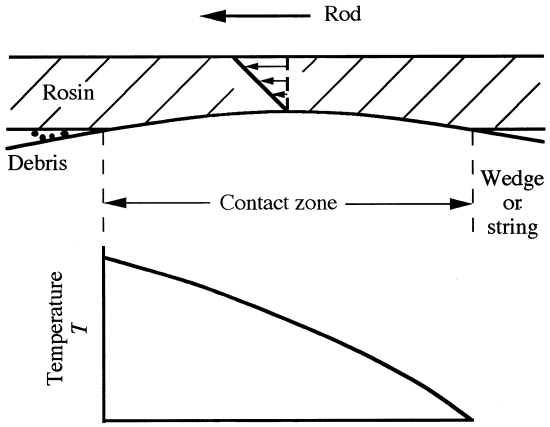

Fig. 14. Sketch of the deforming rosin layer as it passes through the contact zone, showing the velocity profile and temperature variation.

through unit width of this layer will be reduced to one-half the original rate, if the shear is uniform. To accommodate this, presumably some rosin must be squeezed out to the sides or back out of the intake region of the contact.

By the exit of the contact region, the rosin in the active layer will be at its maximum temperature. If this reaches 75°C or so, the rosin will be sufficiently liquid that one might expect slivers or whiskers to be extruded before the adhesive bond to the stationary cylinder was broken. These slivers or whiskers would cool rapidly, become brittle, and break up. This is a possible explanation for the observed accumulation of finely-divided rosin dust in this region on the experimental rig, and indeed in normal playing of bowed-string instruments with a rosined bow.

The friction force, which we wish to calculate, will be the net effect of all processes producing tangential stress. This will include the shearing region, but there may also be contributions from rosin flow out to the sides of the contact zone, and from whisker formation and breakage. To model these processes in detail would require a very elaborate three-dimensional simulation, well beyond the scope of what is intended in this preliminary study. Instead, the assumption will be made that the dominant contribution to the friction force comes from the region of shearing flow. Further, we do not want to take detailed account of the variations of temperature, layer thickness and material properties within the contact region. The objective is to seek the simplest model which goes beyond the usual ad hoc one which allows coefficient of friction to be a function only of instantaneous sliding speed. We therefore work in terms of a single, averaged "contact temperature", T, and a uniform layer thickness δ.

4.5. Temperature calculation

The temperature at the sliding contact can be calculated by modelling the heat generation and transfer in the material surrounding the interface. To summarise, we assume a circular contact area of radius a and an actively-deforming rosin layer of thickness δ. This layer will be considered to be at a uniform temperature T above ambient. One bounding surface, labelled '1', is stationary, while the other, labelled '2', is moving at a speed v. The cylinder of rosin in the deforming contact zone is assumed to be in a state of uniform shear, so that heat generation is uniformly distributed through the volume. The rate at which heat is generated at the contact, Q, is given by the product of the frictional force μN and the sliding velocity:

$$Q = \mu N v \tag{4}$$

This heat input to the contact volume is balanced by three effects: conduction into the two neighbouring solids, convection with the rosin as cold material flows into the contact region while heated material flows out, and absorption in the contact volume, changing its temperature. The first of these effects can be represented in terms of a suitable Green's function for the heat-diffusion problem, while the

other two have simple closed-form expressions within the approximations already stated.

The shearing rosin layer is transported through the contact volume at a mean speed $v/2$. The projected area of the contact volume is $2a\delta$, so the rate of heat transport out of the contact volume is $va\delta\rho_r c_r T$. The mass of the rosin layer at the contact is $\rho_r A\delta$, where ρ_r is the density of rosin. If it is assumed that its temperature rises linearly with an approximately constant effective specific heat capacity c_r, which includes any contribution from change of state, then the associated rate of heat absorption is $\rho_r A\delta c_r \frac{dT}{dt}$. Finally, we deal with the conduction term. The model under development will be used in a time-stepping simulation. At a given time t the past history of the contact temperature T would be known, so the natural formulation is to express the heat flow rate into the bounding surfaces in the form of a convolution integral

$$Q_{\text{cond}} = \int_{-\infty}^{t} g(t-\tau)T(\tau)\,d\tau \tag{5}$$

with a suitable Green's function $g(t)$. Thus the final heat-balance equation is

$$\mu N v = va\delta\rho_r c_r T + \rho_r A\delta c_r \frac{dT}{dt} + \int_{-\infty}^{t} g(t-\tau)T(\tau)\,d\tau. \tag{6}$$

In a homogeneous, isotropic solid with density ρ, specific heat capacity c and thermal conductivity K, the temperature distribution T resulting from a volume heat source q is governed by the diffusion equation:

$$\frac{\partial T}{\partial t} - D\nabla^2 T = \frac{q}{\rho c} \tag{7}$$

where $D\ (= K/\rho c)$ is the thermal diffusivity (Carslaw and Jaeger, 1959). It would be possible in principle to solve this equation for three-dimensional heat flow into two half-spaces to obtain $g(t)$. However, for this initial modelling we will treat the much simpler case of one-dimensional heat flow. To be approximately valid, this relies on the length-scale of temperature variation normal to the sliding contact being short compared with the contact diameter. This requirement will be checked when the model is complete.

4.6. Green's function for one-dimensional heat flow

Even for the one-dimensional problem, the Green's function $g(t)$ requires some care. We begin with the standard result for the temperature response of a semi-infinite rod of cross-sectional area A subjected to a step change of temperature at the end $x = 0$: if

$$T(0, t) = \begin{cases} 0, & t < 0 \\ V, & t > 0 \end{cases}$$

then the subsequent temperature distribution is

$$T(x, t) = V \operatorname{erfc}\left(\frac{x}{2\sqrt{Dt}}\right) \quad t > 0 \tag{8}$$

in terms of the complementary error function (Carslaw and Jaeger, 1959). Thus the heat flow rate into the rod at $x = 0$ is

$$Q = -AK\frac{\partial T}{\partial x}|_{x=0} = \frac{AKV}{\sqrt{\pi Dt}} \quad t > 0. \tag{9}$$

The required Green's function (for flow into one surface only) is the heat flow rate in response to an imposed temperature at $x = 0$ which is a delta function rather than a step, so formally it is the time derivative of this expression. However, the function Q has an infinite discontinuity at $t = 0$, so care must be taken to use the correct time derivative in the sense of generalised functions (Lighthill, 1958). The result has an unfamiliar form, most clearly approached for the present purpose by calculating the discrete-time version which will be needed for a time-stepping simulation. Assume a time step h. Provided the temperature varies only slowly during any single time-period h, the convolution integral (5) is well approximated by

$$Q(mh) \approx \sum_{n=0}^{\infty} g_n T_{m-n} \tag{10}$$

where $T_n = T(nh)$ and

$$g_n = \int_{nh}^{(n+1)h} g(\tau)\, \mathrm{d}\tau. \tag{11}$$

Within this framework, we can take $g(t)$ to be the heat flow in response to an imposed pulse of temperature starting at $x = 0$, of duration h and unit area. The temperature response is then given by the superposition of two terms like Eq. (8), and the required heat flux by a similar superposition of terms like Eq. (9):

$$g(t) = \begin{cases} \dfrac{AKV}{\sqrt{\pi Dt}} & 0 < t < h \\ \dfrac{AKV}{\sqrt{\pi Dt}} - \dfrac{AKV}{\sqrt{\pi D(t-h)}} & t > h \end{cases} \tag{12}$$

with $V = 1/h$. It follows by straightforward integration that

$$g_0 = 2\lambda h^{-1/2},$$

$$g_n = 2\lambda h^{-1/2}\left\{\sqrt{n+1} - 2\sqrt{n} + \sqrt{n-1}\right\} \quad n > 0 \tag{13}$$

where

$$\lambda = \frac{AK}{\sqrt{\pi D}}. \tag{14}$$

Note that when $n \gg 1$,

$$g_n \approx -\frac{\lambda}{2h^{1/2}n^{3/2}} \tag{15}$$

which is what would be expected from the normal functional derivative of Eq. (9) with respect to t.

The discrete Green's function given by Eq. (13) looks quite peculiar, because of the $\sqrt{h}$ factors which appear in it. The "continuum" limit $h \to 0$ apparently does not give anything sensible. However, numerical experiments have confirmed that convolutions of this function with well-behaved functions do indeed give results which are stable as $h \to 0$. One desirable feature is immediately apparent: $\sum_n g_n$ converges to zero as the sum is taken to infinity, corresponding to the fact that when a steady temperature is imposed at $x = 0$ for a long time, the heat flux there tends to zero since the temperature gradient becomes arbitrarily small. All the terms except g_0 are negative, so this result relies entirely on the anomalous value of g_0. The case of steady sliding, and hence steady temperature at $x = 0$, will be important in the next stage of development of the model.

For the stationary surface, we can use this discrete Green's function directly to calculate the heat flow into it given the history of the contact temperature. Parameter values K_1, D_1 and λ_1 are used for this surface, and the resulting values from Eq. (13) are denoted $g_n^{(1)}$. The same Green's function can also be used to describe heat flow into the moving surface, using values K_2, D_2 and λ_2 and denoting the result $g_n^{(2)}$. However, the convolution integral should now be restricted to a short period of the temperature history, corresponding to the average time that a point on the moving surface has been in the contact region. At steady speed v the transit time for a point to cross the contact region, averaged with respect to area, is $16a/3\pi v$. The "average" point has thus been within the contact region for a time $8a/3\pi v$, and the upper limit for the sum in Eq. (10) becomes

$$n_{\max} = 8a/3\pi vh \tag{16}$$

for the moving surface. When v is time-varying, a corresponding upper limit can be based on the average time a point on the centre-line of the contact has been within the contact region. The final discrete form of the convolution integral from Eq. (6) is then

$$\sum_{n=0}^{\infty} g_n^{(1)} T_{m-n} + \sum_{n=0}^{n_{\max}} g_n^{(2)} T_{m-n}. \tag{17}$$

This average transit time also gives a simple way to examine the validity of the

assumption of one-dimensional heat flow. The typical depth to which a heat disturbance penetrates in time t is $2\sqrt{Dt}$, from Eq. (8). If we use the transit time in this expression, then the one-dimensional assumption seems reasonable for the moving surface if this scale depth is small compared to the average transit distance across the contact. This condition leads to the requirement

$$v \gg \frac{3\pi D}{4a}. \tag{18}$$

For wood or perspex surfaces sliding in the stick–slip rig, assuming a typical contact radius of 0.4 mm, this threshold for v is of the order of 1 mm/s. The heat flow at the contact is therefore one-dimensional to a good approximation under the conditions used in the tests reported earlier, in which mean sliding speeds were typically greater than 20 mm/s. This argument does not apply to the stationary surface, but in that case the material immediately below the surface will have time to reach a rather uniform temperature so that the heat flow into it will be low compared to that into the moving surface. Small errors in the exact magnitude of this heat flow may not affect the overall heat balance very much. The effect of any relatively rapid transient fluctuations of temperature will be correctly represented, since the one-dimensional assumption would then be valid again.

5. Friction models

5.1. Viscous model for steady sliding tests

We now seek a simple constitutive law for the relevant material properties of rosin in which T will be allowed to enter as a state variable. If a continuous film of viscous liquid is formed at the interface and this is able to support the normal load, the frictional force would arise entirely as a result of the viscous shearing of the layer. This model is the natural one to investigate first, in the light of the rheometer tests which showed essentially viscous behaviour over the range of temperature, strain and frequency tested. The simplest constitutive law would be to treat the molten layer as a Newtonian fluid with a temperature-dependent viscosity $\eta(T)$ satisfying Eq. (3). The shear strain rate is v/δ, so the friction force is then given by

$$\mu N = \eta A v/\delta \quad \text{(viscous model)} \tag{19}$$

where the contact area $A = \pi a^2$.

The simplest and most reliable of the rosin friction measurements reported in Section 3 is of the variation of coefficient of friction with speed during steady sliding. We can use these results to give information about the as yet undetermined layer thickness δ and contact radius a. We expect δ to be of the order of a few microns (based on the micrographs), and a to be of the order of a few hundred microns (based on Hertz theory and direct observation). If sliding

speed and temperature are constant, then Eq. (6) reduces to a very simple form. The dT/dt term is absent, and the heat flow into the stationary surface is zero. Thus

$$\mu N v = va\delta\rho_r c_r T + T\sum_{n=0}^{n_{\max}} g_n^{(2)} \approx va\delta\rho_r c_r T + TAK_2\sqrt{\frac{3v}{8aD_2}} \tag{20}$$

using Eqs. (13), (14) and (16).

Eq. (20) is to be combined with the viscous constitutive law (19), the measured temperature–viscosity relation for rosin, Eq. (3), and the curve-fitted approximation to the measured coefficient of friction, Eq. (2) and Fig. 4. Eliminating temperature and viscosity between these equations leaves a nonlinear algebraic relation between v, a and δ. This can be solved numerically, using appropriate values for the other parameters. The steady-sliding experiment was performed using a rosin-coated perspex rod sliding over a perspex wedge, with a normal force of 3 N. Relevant thermal properties of perspex and rosin are given in Table 1. The result of this calculation is shown in Fig. 15(a), as a plot of a as a function of v and δ. The range of δ is governed by the fact that the whole layer of rosin is estimated to be at most 30 μm thick, so the deforming layer cannot be thicker than this. The associated contact temperature T is plotted in similar fashion in Fig. 15(b).

From the behaviour of rosin described earlier, we might expect that this viscous model would apply most plausibly if the temperature was around 55° above ambient. Much below that and the deforming layer would be rather rigid, while above that one would expect the high temperature to result in the "melted" layer penetrating deeper in the rosin (unless the full depth was already melted). From Fig. 15(b) we can deduce that as the sliding speed rises from 0 to 0.11 m/s, the layer thickness increases from 0 to about 30 μm (or to the full depth, whichever is less). From Fig. 15(a), the contact radius would then range from about 0.27 mm up to about 0.37 mm, a modest range of values in line with expectations. The calculation can, of course, be repeated with different normal loads. For example, with a normal force of 6 N the thickness ranges from 0 to 30 μm as sliding speed rises from 0 to 0.09 m/s, while the radius ranges from 0.42 to 0.59 mm.

It should be noted in passing that the dependence of the frictional force on normal load arises purely as result of the dependence of the contact area A on the normal load. To obtain a true coefficient of friction, independent of normal load, A must be directly proportional to normal load N. On the other hand, if we use the relation for Hertzian contact we obtain $A \propto N^{2/3}$. The experimental results suggest that the coefficient of friction is not strongly dependent on the normal load. A possible rationalisation would be that the experiments were operating close to the seizure load, so that the normal load was supported by a process of yield operating over the whole contact area, requiring $A \propto N$.

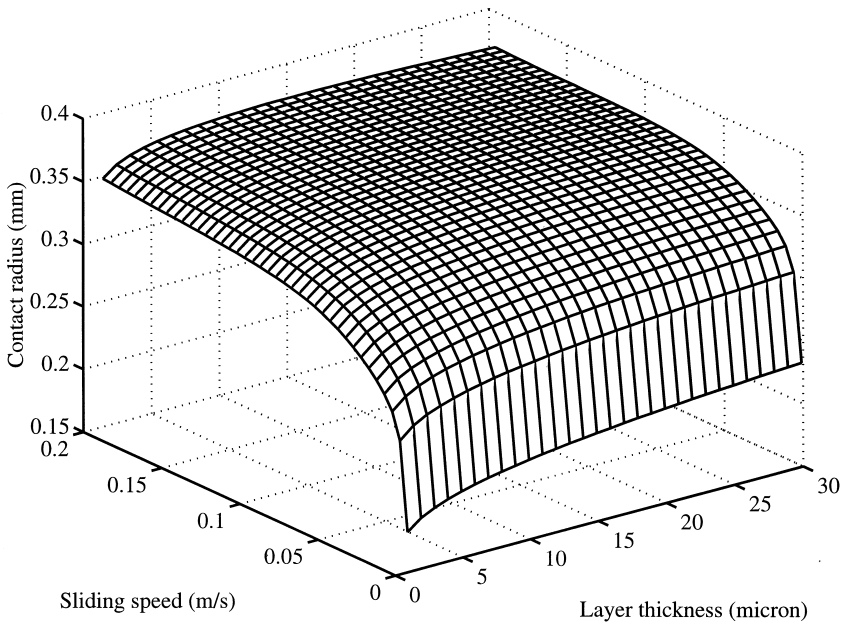

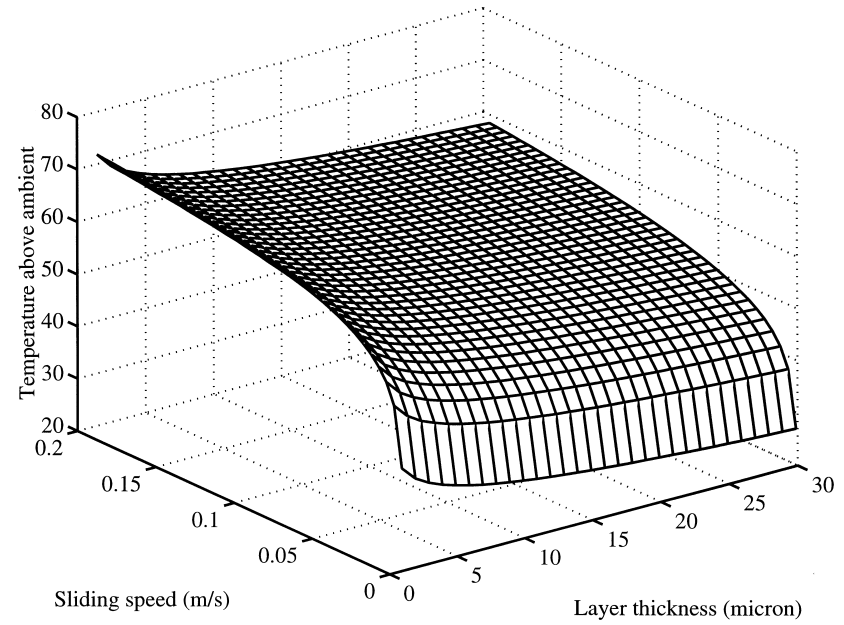

Fig. 15. (a) Contact radius as a function of sliding speed and layer thickness, for steady sliding within the viscous model for rosin behaviour. (b) Contact temperature as a function of sliding speed and layer thickness, for steady sliding within the viscous model for rosin behaviour.

5.2. Viscous model for sinusoidal sliding

The next set of experimental results to be considered was obtained during forced sinusoidal sliding at a frequency of approximately 4 Hz. Some observed friction/velocity characteristics were shown in Fig. 5. The coefficient of friction showed significant hysteresis, one side of these hysteresis loops following the steady-sliding relation fairly closely while the other side gave lower values of friction. It seems plausible that this hysteresis might be the result of thermal inertia, in the context of the present model.

To simulate this experiment, it is necessary to use the full time-varying form of the heat balance Eq. (6). A discrete time step h is chosen, and the derivative $\mathrm{d}T/\mathrm{d}t$ is approximated by a first-order forward difference. At each time step, this equation can then be used to give the new temperature in terms of the previous value, the corresponding values of friction force calculated via the constitutive law (19) and the heat flow into the substrate materials given by the convolution (17). Numerical experiments show that provided a sufficiently small time step h is chosen, the results are stable, and converge to a limiting form of behaviour as h is reduced.

In the spirit of the model being tested, a simplifying assumption is now necessary. In the case of steady sliding, there is time for the contact conditions (temperature, radius and thickness) to adjust to their equilibrium values. However, in a time-varying situation one would not expect this adjustment to be complete, since the time scale for heat diffusion is rather long. To model the physics of this process realistically would go, once again, beyond the scope of this study. The simplest remedy is to suppose that the layer thickness and radius remain essentially constant, at values appropriate to the RMS sliding speed, say. The temperature in the deforming layer will then fluctuate in response to the varying sliding speed. This assumption seems somewhat plausible for the present case of oscillatory sliding at 4 Hz, and becomes more plausible when we turn to consider stick–slip oscillations at significantly higher frequencies.

The two tests for which we seek comparison were as follows. In the first, the normal load was 3 N and the peak sliding speed was about 0.08 m/s, so that the RMS value was approximately 0.05 m/s. For steady sliding at this RMS speed with a contact temperature of 75°C (i.e. 55° above ambient), the contact radius should be 0.35 mm (from Fig. 15(b)) and the layer thickness 10 μm (from Fig. 15(a)). The second test had a peak sliding speed around 0.19 m/s, so an RMS value 0.14 m/s, requiring a contact radius 0.37 mm and a layer thickness 30 μm. A time step of 20 μs was used for the simulations.

The simulated results obtained with these parameter values are shown in Fig. 16, for comparison with the measurements in Fig. 5. In both cases the contact temperature ranged between about 42 and 59° above ambient. The simulated results are similar in many respects to the measured ones. The steep but finite slope in the friction/velocity characteristic corresponding to the "sticking" region near zero sliding speed is rather well matched. The fairly close following of the steady-sliding characteristic at relatively high sliding speeds is reproduced. The

fact that the maximum coefficient of friction is higher in Fig. 5(a) and (b) than in Fig. 5(e) and (f) is reproduced. The width of the sharp spike following each point of zero speed in the time history of the coefficient of friction is quite well matched. The one feature which is obviously not well reproduced is the magnitude of the hysteresis. The simulation predicts coefficients of friction which rise well above the steady-sliding curve just after "sticking", whereas the measurements show maximum values comparable with the steady-sliding curve. The overall conclusion, though, is that this model seems very promising.

5.3. The plastic model

To assess the model quality further, it is useful to have an alternative with which to compare and contrast it. The viscous model was motivated by imagining an interfacial layer sufficiently hot to behave as a liquid. If, however, the interfacial layer only heats up to a more modest level, the viscosity would be so

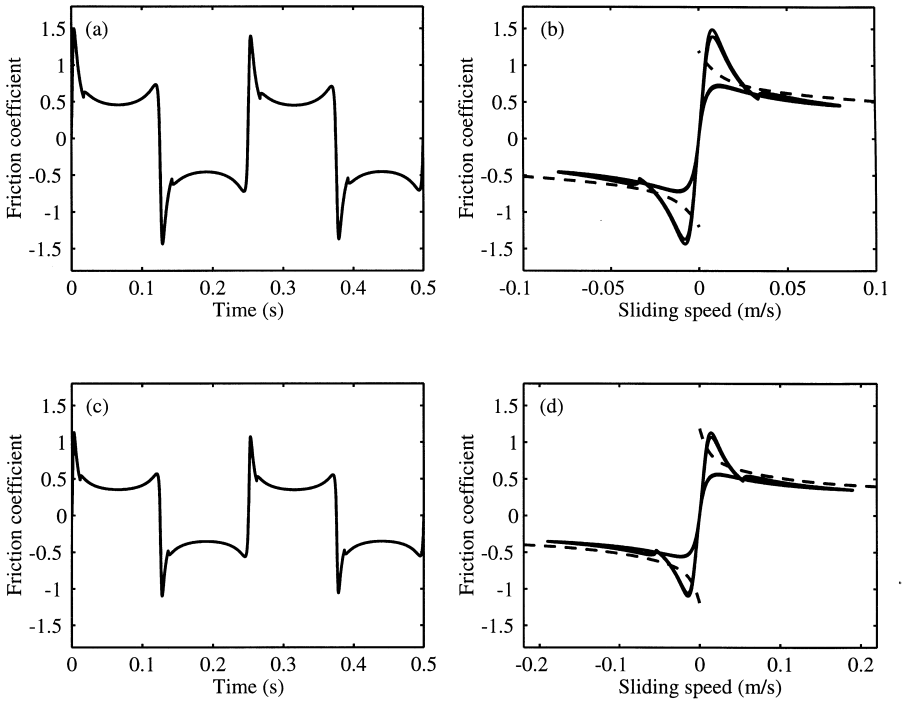

Fig. 16. Frictional response to forced sinusoidal sliding, as a function of time and sliding speed: (a–b) behaviour simulated using the viscous model, with a contact radius 0.35 mm, layer thickness 10 μm, peak sliding speed 0.08 m/s and normal force 3 N, for comparison with Fig. 5(a) and (b); (c)–(d) behaviour simulated using the viscous model, with a contact radius 0.37 mm, layer thickness 30 μm, peak sliding speed 0.19 m/s and normal force 3 N, for comparison with Fig. 5(e) and (f).

high, according to the measurements shown in Fig. 12, that one might expect the rosin to behave more or less as a solid. The friction force would then be governed by a different kind of interfacial process. The rosin near the sliding interface might behave as a viscoplastic solid, and a rigid/plastic model might be contemplated in which the shear stress was a function of temperature only, independent of the shear strain (except that the sign of the strain governs the sign of the friction force). Then

$$\mu N = A k_y(T)\mathrm{sgn}(v) \quad \text{(plastic model)} \tag{21}$$

where k_y is the shear yield stress. This model is equivalent to retaining the notion of a coefficient of friction, but treating it as a function of temperature rather than of sliding speed. Under the conditions of the measurements reported above, plastic flow of the surface layer of the rosin is quite plausible. The normal force was typically of the order of a few Newtons, and the contact radius a few tenths of a millimetre. This leads to stresses of the order of tens of megapascals, roughly the expected magnitude of the shear yield stress of a material whose shear modulus is of the order of a gigapascal.

With this model, the rheometer measurements do not give any guidance as to the appropriate form of the function $k_y(T)$. Instead, we can use the steady-sliding measurements directly as a form of calibration (provided we assume that those experiments were also in a regime where this model is appropriate). Eq. (20) for steady sliding is still appropriate, and it can be inverted to give the function $T(v)$ from the measurement of the function $\mu(v)$. On the other hand, Eq. (21) gives the function $k_y(v)$, and combining the two gives a parametric expression for the required function $k_y(T)$. Carrying this calculation through, the required variation of yield stress with temperature is shown in Fig. 17(a) for a variety of values of contact radius a and a layer thickness $\delta = 1$ μm. The top curve assumes a radius 0.2 mm, and the remaining curves assume radii rising in steps of 0.05 mm until the lowest curve which assumes a radius 0.5 mm. Fig. 17(b) shows the corresponding results for a layer thickness of 30 μm. In all cases the curves have a similar shape, falling from an initial value by a factor of 3 or so to an asymptotic constant value at higher temperatures.

It is immediately apparent that the layer thickness has very little influence on the behaviour. This can be traced back to the rather small value for the specific heat of rosin used here, small enough that the convective term in Eq. (20) is negligible (given the other parameter values in use). This term is the only place that the layer thickness enters the steady-sliding calculation. However, it should be noted that this value for the specific heat comes from the work of Cobbold and Jackson (1992), who do not attribute very great accuracy to it. Apparently comparable materials such as paraffin wax have much higher values. If the value were found to be bigger by a significant factor (3 or more), the convective term, and hence the layer thickness, would have a more marked influence on the results.

This model can be used to simulate the sinusoidal excitation experiment, with any particular assumed values of a and δ. Without a detailed three-dimensional

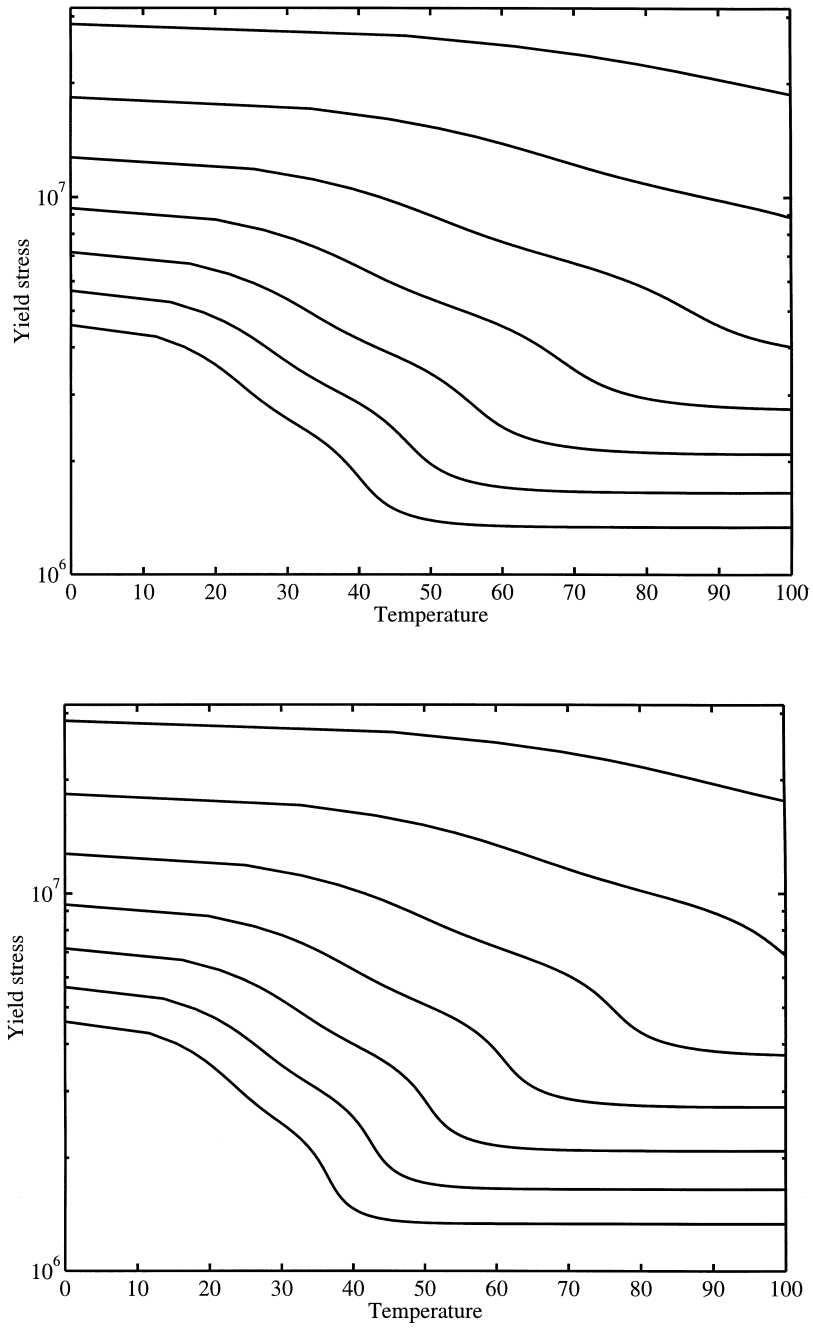

Fig. 17. Shear yield stress k_y deduced from the steady-sliding measurements, as a function of temperature above ambient, for a layer thickness (a) 1 μm; (b) 30 μm. Top curves: contact radius 0.2 mm; successive curves at 0.05 mm intervals until bottom curves: radius 0.5 mm.

heat-flow calculation, there is no obvious basis for selection of correct values of these parameters, except that for plausibility the maximum contact temperature should remain low enough for the rosin to behave as a solid. Some representative results are shown in Fig. 18. Using the values $\delta = 10$ μm, $a = 0.5$ mm the friction/velocity characteristic is as shown in Fig. 18(b), while as shown in Fig. 18(a) the temperature remains below 40° above ambient (60°C), probably low enough for plausibility of this model. Other parameters used here are the same as for Fig. 16(a) and (b), and Fig. 18(b) is directly comparable with Figs. 5(b) an(d) 16(b). Fig. 18(c) was computed with the same parameter values except for a higher peak sliding speed, and is directly comparable with Figs. 5(f) and 16(d).

To assess the significance of these (rather arbitrary) choices of radius and thickness, Fig. 18(d) shows the friction/velocity characteristic resulting from the same parameter set as Fig. 18(b) except for a significantly different choice of radius, $a = 0.25$ mm. (Recall that thickness is expected to have little influence.) The contact temperature in this case ranged between 75 and 115°C above ambient, far too high for plausibility of this model, but the friction behaviour can

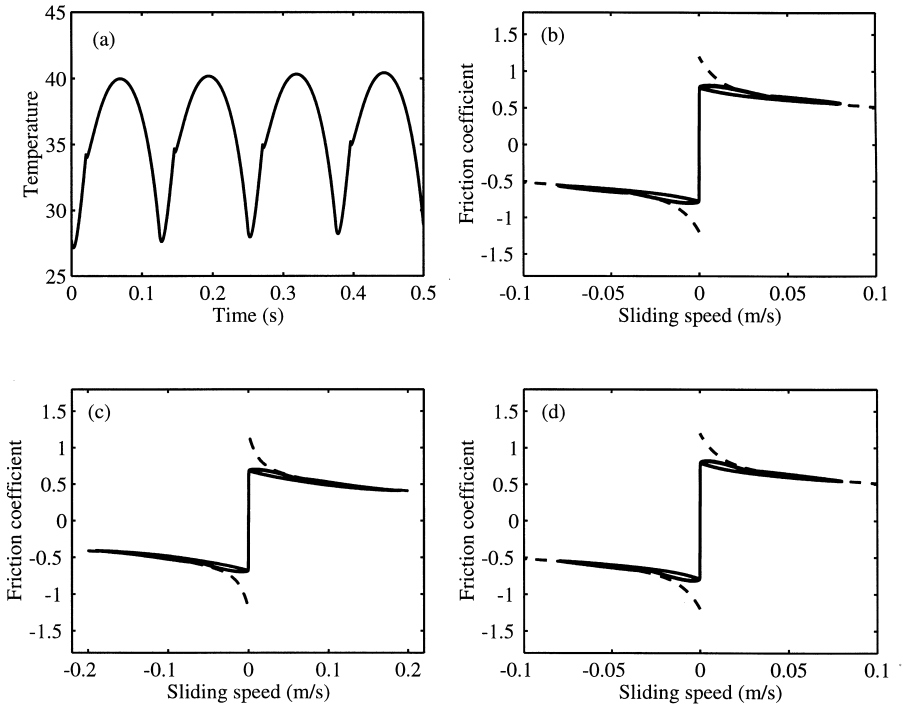

Fig. 18. Frictional response to forced sinusoidal sliding, simulated using the plastic model of rosin behaviour: (a) temperature variation with normal force 3 N, peak sliding speed 0.08 m/s, radius 0.5 mm and layer thickness 10 μm; (b) friction/velocity characteristic for the same conditions; (c) friction/velocity characteristic with peak sliding speed 0.19 m/s; (d) as (b) but with radius 0.25 mm.

be seen to be extremely similar. This is a very reassuring result: using the steady-sliding friction measurements to calibrate the model, and then predicting the results of sinusoidal sliding, seems to produce a result which is very insensitive to the choice of these parameter values, except for the prediction of absolute temperature levels. Any value which produce acceptably low temperatures leads to very similar frictional behaviour, so that we can have some confidence that a comparison between, for example, Fig. 18(b) and the measurement shown in Fig. 5(b), is meaningful.

The results of this "plastic" model differ from those of the viscous model in several details. The term $\mathrm{sgn}(v)$ in Eq. (21) means that the "sticking" portion of the characteristic is truly vertical, since the force changes sign instantaneously when the velocity passes through zero. This abrupt reversal also guarantees that the magnitude of the friction force is the same immediately before and immediately after the reversal. The model does show slight hysteresis, in the same sense as the viscous model and the measurements, but it takes the form of two separate loops which close at the limits of the vertical line. The hysteresis loops in this case are smaller than the observed ones (Fig. 5(b) and (f)), whereas the corresponding predictions of the viscous model gave loops which were appreciably bigger than the observed ones.

A point of similarity of both models and the measurements is that the hysteresis loops are largely confined to sliding speeds close to zero. The friction coefficient always shows a rise followed by a marked dip, and for higher sliding speeds it traces out much the same curve for rising and falling speed. This rise and marked dip manifests itself in different details in the two models, but the width is very similar in both. It is associated with the temperature variation, largely independent of the precise details of the constitutive law. The fact that clearly similar features can be seen in the measurements is strong evidence that contact temperature is indeed implicated in the real frictional behaviour, the central claim of this study.

6. Modelling stick–slip motion

6.1. Simulation method

In order to simulate the stick–slip measurements, it is first necessary to model the dynamics of the cantilever structure used as the oscillator. The design of this cantilever, shown in Fig. 3, may be approximated by a massless strip of length l clamped at one end, carrying a rigid "head" at its free end, as shown in Fig. 19. Let the head have a mass m and a moment of inertia I_G about its centre of mass, distant a from the end of the strip. This idealised system has two degrees of freedom, with the rigid head undergoing translation z at the end of the strip, and rotation θ, say. Since the flexible strip is massless its deformed shape will be governed by static equilibrium. Imposing clamped boundary conditions at $x = 0$ and the given displacement and rotation at $x = l$ yields the displacement shape:

$$y = \frac{3z - l\theta}{l^2}x^2 + \frac{l\theta - 2z}{l^3}x^3 \tag{22}$$

with the coordinates x and y indicated in Fig. 19.

Applying Lagrange's method to the cantilever now yields the following eigenvector equation for the two normal modes of the system:

$$\frac{2EI}{l^3}\begin{bmatrix} 6 & -3l \\ -3l & 2l^2 \end{bmatrix}\begin{bmatrix} z \\ \theta \end{bmatrix} = \omega^2\begin{bmatrix} m & ma \\ ma & ma^2 + I_G \end{bmatrix}\begin{bmatrix} z \\ \theta \end{bmatrix} \tag{23}$$

where E is the Young's modulus and I is the second moment of area of the flexible portion of the cantilever. The eigenvalues of this equation are a close approximation to the frequencies of the first and second bending modes of the experimental cantilever when the following parameter values are used: $E = 3.0$ GPa, $I = 60$ mm^4, $m = 20$ g, $I_G = 4.0 \times 10^{-6}$ kg m^2, $l = 18.5$ mm, $a = 22.5$ mm. The two mode shapes derived using the parameters above are shown (with an exaggerated transverse scale) in Fig. 19.

It is useful to describe the cantilever dynamics by a Green's function, so that the dynamic simulation can be carried out by convolution. To calculate the displacement of the cantilever at point c (the accelerometer position) when a force

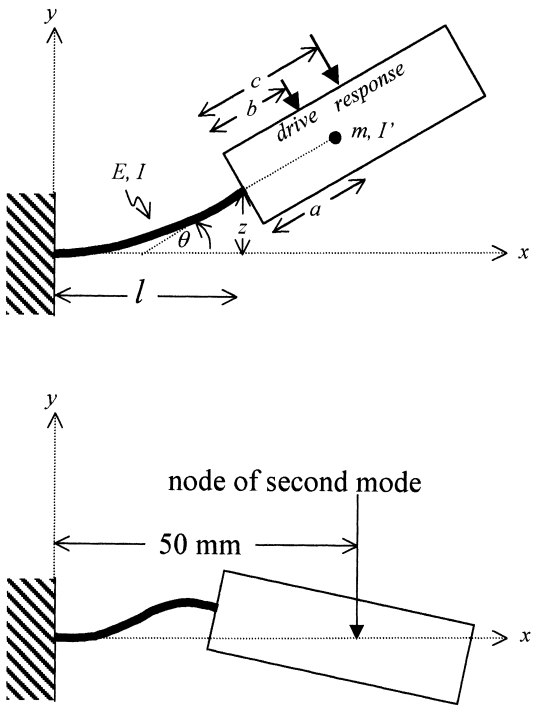

Fig. 19. Sketch of mechanical model of cantilever, indicating the form of the two vibration modes.

$f(t)$ is applied at point b (the point of contact), the following integral is required:

$$x(t) = \int_0^t g(b, c, t')f(t - t')\,\mathrm{d}t' \tag{24}$$

where the Green's function $g(b, c, t)$ is the displacement response of the cantilever at point c to a force impulse delivered at point b. In general, the Green's function for an N degree-of-freedom system with light damping can be expressed as (Skudrzyk, 1968):

$$g(b, c, t) = \begin{cases} 0 & t < 0 \\ \sum_{n=1}^{N} \dfrac{\phi_n(b)\phi_n(c)}{\omega_n} \sin(\omega_n t)\mathrm{e}^{-\lambda_n t} & t \geq 0 \end{cases}. \tag{25}$$

In this expression ω_n and λ_n are the angular frequency and damping factor of the nth mode, whose mass-normalised mode shape is ϕ_n. In terms of Q-factors, $\lambda_n = \omega_n/2Q$ for light damping. For the present problem a value $Q = 20$ is appropriate for both modes.

Stick–slip simulation now requires a time-stepping procedure. A time step h is chosen. At each time step the contact temperature is calculated by the procedure described in Sections 4 and 5, involving a convolution integral with the temperature history to compute the rate of heat conduction into the substrate materials. From the temperature and an assumed constitutive law the friction force can be calculated. Finally, integral (24) can be evaluated using the force history to give a new value for the displacement (or velocity or acceleration if desired, using appropriate modified Green's functions). For this purpose we require that b and c coincide, since the motion is required at the point of application of the friction force. The results are stored, and the calculation proceeds to the next time step.

Using the simplest approach to the convolution (24), the number of terms to be summed would increase as the simulation proceeds, to the detriment of both speed and accuracy. However, the particular form of the Green's function for this problem allows a more efficient procedure to be used. Eq. (24), when expressed in discrete form with the time increment h, can be written

$$g(nh) = \mathrm{Re}(g_1\alpha_1) + \mathrm{Re}(g_2\alpha_2) \tag{26}$$

where

$$g_j = \phi_j(b)\phi_j(c)/\omega_j, \qquad \alpha_j = \exp(i\omega_j h - \lambda_j h) \quad j = 1, 2. \tag{27}$$

Write

$$x_k = x(kh), \qquad f_k = f(kh) \tag{28}$$

Then Eq. (24) may be approximated in the compact form

$$X_{k+1}^{(j)} = -ig_j f_{k+1} h + \alpha_k X_k^{(j)}, \quad j = 1, 2 \tag{29}$$

with

$$x_k = \mathrm{Re}\left(X_k^{(1)} + X_k^{(2)}\right). \tag{30}$$

6.2. The friction-curve model

Before showing results of simulation using the proposed new constitutive laws, it is useful to have for comparison the results using the traditional model. For this, we may use the friction characteristic found by curve-fitting to the measurements obtained during steady sliding, Eq. (2). To use this model the time-stepping procedure is simpler than the one just described, since it is not necessary to calculate the temperature. At each time step the velocity at the contact point is determined as just described, then the friction force at that time deduced from the assumed friction/velocity law.

To model the indeterminacy of friction during the sticking phase of the motion, it is convenient to replace the infinite slope of the ideal stick/slip model with a finite slope. A convenient way to do this is to modify the curve-fitted friction law to the form

$$\mu = \left\{0.4\exp(-|v_\mathrm{b} - v|/0.01) + 0.45\exp(-|v_\mathrm{b} - v|/0.1) + 0.35\right\} \times \frac{2}{\pi}\tan^{-1}\left(\frac{v_\mathrm{b} - v}{v_0}\right). \tag{31}$$

The function $\frac{2}{\pi}\tan^{-1}(\frac{v_\mathrm{b}-v}{v_0})$ replaces the Heaviside step function of the idealised law, and by choosing the value of the constant v_0 the precise shape of the function can be adjusted. The value 0.0002 has been used for computations, small enough that the curve is only modified at speeds lower than any of the data points on which the curve-fit was based.

To illustrate, we simulate the example of stick–slip measurements shown in Fig. 6. The parameter values were: normal load $N = 6$ N, sliding speed $v_\mathrm{b} = 0.042$ m/s. When this experiment is simulated using the constitutive law of Eq. (31), the result is as shown in Fig. 20. A time step $h = 1.5$ μs was used to ensure convergence. Stick–slip motion is indeed predicted, at approximately 34 Hz compared with 60 Hz in the measurement. The velocity waveform is qualitatively similar to that in Fig. 6(b), except that to compensate for the longer sticking intervals the peak sliding speed is higher. Recall that the ripples visible during the nominal sticking phase in the measured waveforms are caused by the fact that the accelerometer could not be placed exactly at the contact point, so that some signal from the second vibration mode of the cantilever is picked up. These ripples do not influence the contact behaviour and should be ignored when comparing with simulated waveforms, for which it is of course possible to show the motion of the exact contact point.

The principal difference between the measured and simulated results is then seen in the acceleration waveforms at the transition from slipping to sticking. The simulations show a rise to a very sharp peak immediately before sticking is initiated, in contrast to the measurements which show a much smoother variation and a lower peak value. This deviation is associated with the observed hysteresis in the friction/velocity plane which was discussed at length earlier. The simulation has no hysteresis, of course.

6.3. The viscous model

The challenge for the thermally-based models is to produce simulated waveforms which more closely match the observations. The investigations of Section 5 suggested that the viscous constitutive law might be the most appropriate, and this is tested next. The heat-flow model on which the simulation is based requires a value for the radius and thickness of the "melted" layer of rosin in the contact region. Plausible values for these parameters were determined by requiring that the contact temperature would be around 55° above ambient (i.e. 75°C) during *steady* sliding at the assumed rod speed. Using the results shown in Fig. 15, the relevant values are: thickness = 8 μm, contact radius = 0.53 mm.

The results of simulation with these values, shown in Fig. 21, can only be described as disastrous. Although quasi-periodic motion is predicted, it has a very long time scale and waveforms which bear no resemblance to the observations. The velocity v of the oscillator is predicted to rise, on occasions, to a value approaching 1 m/s, much faster than the rod. In frictional terms this would be

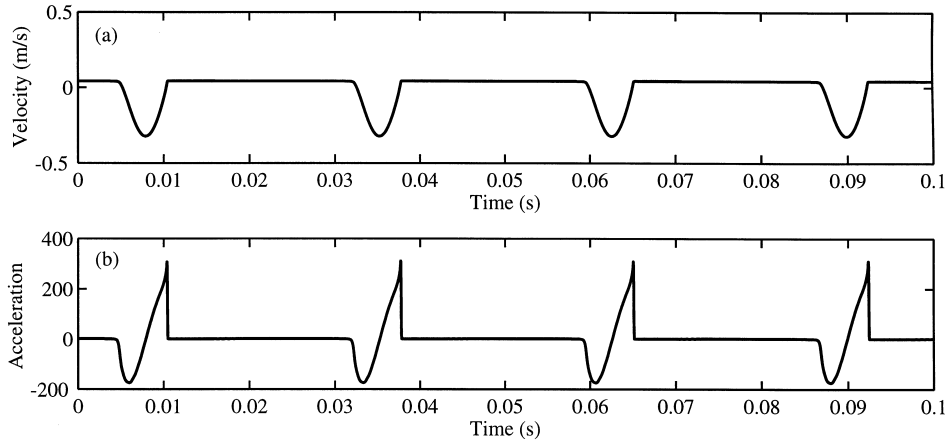

Fig. 20. Simulation of stick–slip motion using the oscillator model and the traditional frictional law depending on sliding speed according to Eq. (31). Rod speed and normal force were as for Fig. 6. Velocity (a) and acceleration (b) waveforms comparable to Fig. 6, except that the vertical scales are different.

described as "forward slipping" (although this model does not distinguish "sticking" and "slipping" states).

The viscous model does not look promising based on these results, but before rejecting it completely it is worth considering a different case. As was noted above, the values for the thermal properties of rosin used in this study were those given by Cobbold and Jackson (1992). Those authors pointed out that their determination of the diffusivity, and hence the specific heat capacity, was not very accurate. The value they give, 250 J/kg/K, seems unexpectedly low. Values listed for apparently comparable materials such as paraffin wax are an order of magnitude higher (Kaye and Laby, 1986). As an experiment, the simulation was re-run using a value for specific heat capacity of 2884 J/kg/K. The calculation for the contact geometry then yields a thickness 30 μm and a radius 0.43 mm.

The results are shown in Fig. 22. This time something much more like stick–slip motion is predicted. The frequency is very low, approximately 19 Hz. The acceleration waveform shows a very smooth form, certainly lacking the very sharp spike at the end of slipping seen in Fig. 20. The contact temperature varies between 40 and 60° above ambient, a fairly plausible range for consistency with

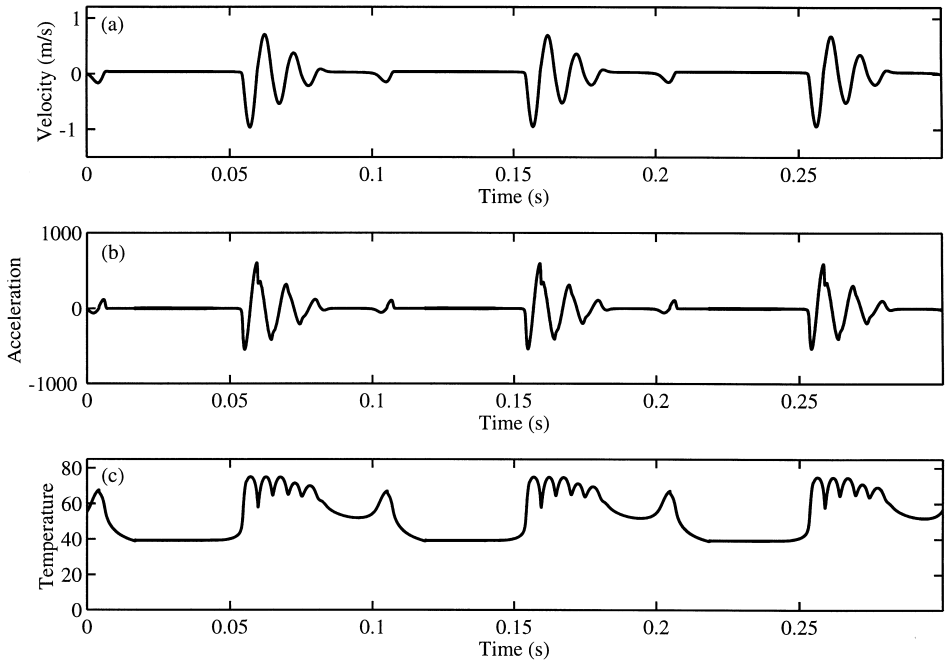

Fig. 21. Simulation of stick–slip motion using the oscillator model and the viscous frictional law depending on contact temperature, using rosin properties as listed in Table 1. Rod speed and normal force were as for Fig. 6. Velocity (a) and acceleration (b) waveforms are comparable to Fig. 6, but both horizontal and vertical scales are different. Temperature (c) is relative to ambient (assumed to be 20°C).

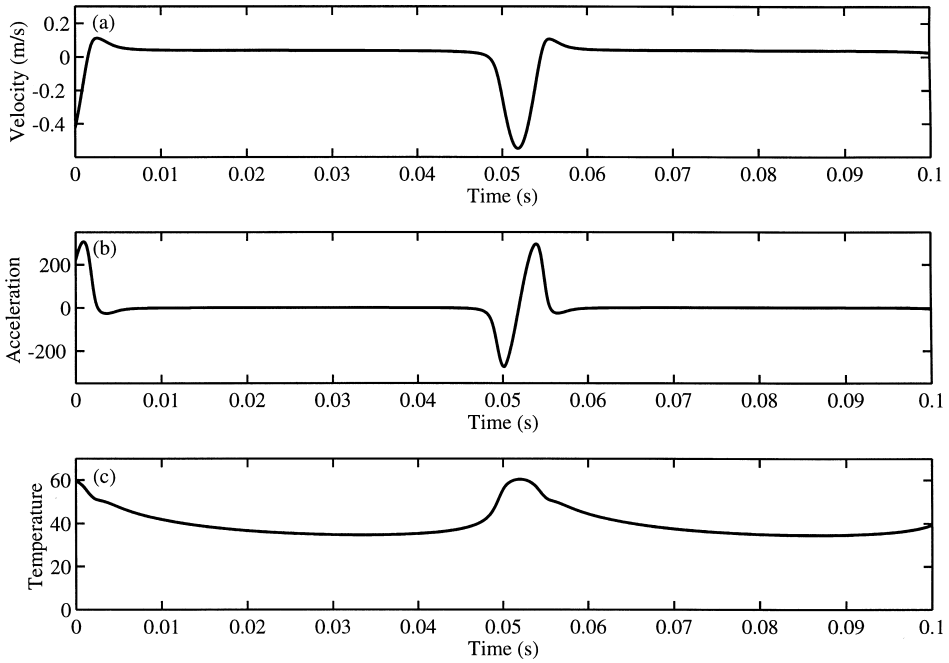

Fig. 22. Simulation of stick–slip motion using the oscillator model and the viscous frictional law depending on contact temperature, using parameter values as for Fig. 4 but with the specific heat capacity of rosin increased to 2884 J/kg/K. Velocity (a), acceleration (b) and temperature (c) plotted on the same horizontal scale as Figs. 6 and 20.

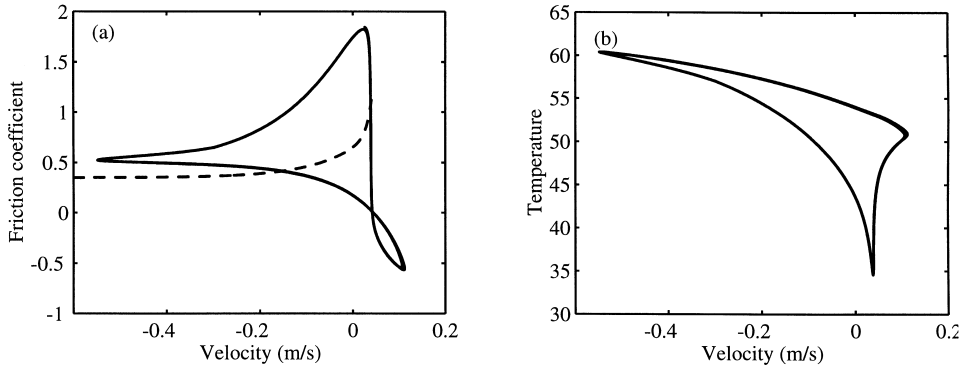

Fig. 23. Coefficient of friction versus oscillator velocity (a) and contact temperature versus sliding velocity (b), for the simulated stick–slip motion shown in Fig. 22. The friction/velocity characteristic from steady sliding measurements is shown in (a) as a dashed line.

the assumptions of the viscous model. The corresponding friction/velocity and temperature/velocity plots are shown in Fig. 23. A substantial hysteresis loop is seen in the friction/velocity plane, in the same sense as the observed loops but not showing good agreement in shape or size. The origin of this hysteresis lies in the time lag arising from thermal inertia, as is made explicit in Fig. 23(b). The friction force is governed by the temperature, but the temperature is not a single-valued function of velocity: again a hysteresis loop is seen, which is traversed in a clockwise sense.

Although these results using the "wrong" specific heat look more plausible than those with the "right" value, they are still clearly unsatisfactory. Similar simulations have been run with a wide variety of parameter values, and they all show the feature of "forward slipping". During an episode of sliding the rosin layer heats up, so that towards the end of the sliding episode the viscosity is low. There is then insufficient force available for the oscillator to be "recaptured" by the rod for a new sticking episode without some overshoot occurring. This is evident in Fig. 22(a), and causes the obvious feature in the lower right-hand corner of Fig. 23(a), whereas nothing like this is ever seen in the experimental results. We conclude that the viscous constitutive model does not give a good representation of the physical behaviour of rosin during these self-excited oscillations, even though it had performed quite well in simulating the case of forced sinusoidal sliding.

6.4. The plastic model

We now turn to the alternative constitutive model proposed earlier. If the contact temperature does not rise into the "melting" range, then the behaviour might be better described in terms of interfacial plastic yielding. The yield stress would be expected to vary with temperature, and a method was described earlier for inferring an appropriate functional variation of this yield stress from the experimental results on steady sliding. The constitutive law to be used here can be written

$$\mu = \frac{Ak_y(T)}{N} \times \frac{2}{\pi}\tan^{-1}\left(\frac{v_b - v}{v_0}\right) \tag{32}$$

which is Eq. (21) modified by a factor as in Eq. (31) to smooth the jump near zero speed, for numerical stability. The numerical value $v_0 = 0.0002$ is used, as before.

Unlike the viscous model there is no independent calibration measurement for this model, so that there is no clear-cut method to estimate the layer thickness and contact radius. However, it was found before that the heat-flow calculation was insensitive to the layer thickness. Also, from Eq. (32), if both μ and k_y are to be regarded as material properties, then the contact area must vary in proportion to the normal load. This assumption can be rationalised by supposing that the interfacial area is sufficiently soft that the real area of contact is equal to the

apparent area of contact because the asperities have all been flattened. With these points in mind, the parameter values chosen for simulation were: layer thickness $\delta = 10$ μm, contact radius $a = 0.3\sqrt{N}$ mm.

The result of a simulation of the standard case, corresponding to Figs. 6 and 20–22, is shown in Fig. 24. The friction/velocity and temperature/velocity plots, corresponding to Fig. 23, are shown in Fig. 25. For this simulation a time step $h = 5$ μs was used. This value ensured convergence of the velocity waveforms, but gave a somewhat noisy acceleration waveform due to the rapid force variation near sticking. The waveform has been smoothed slightly in the version plotted here, for clarity.

This time the velocity and acceleration waveforms show stick–slip motion at about 44 Hz, whose details match the measurement reasonably well. Note that this figure has the same vertical scalings as Fig. 6, whereas Figs. 20–22 required different scaling. The contact temperature fluctuates in the range 20–40° above ambient, low enough for reasonable self-consistency with the assumption of the plastic model. The friction/velocity curve shows an anticlockwise hysteresis loop quite similar to that seen in the measurements, and in particular it departs from the steady-sliding curve (shown as a dashed line) in very much the same way. The

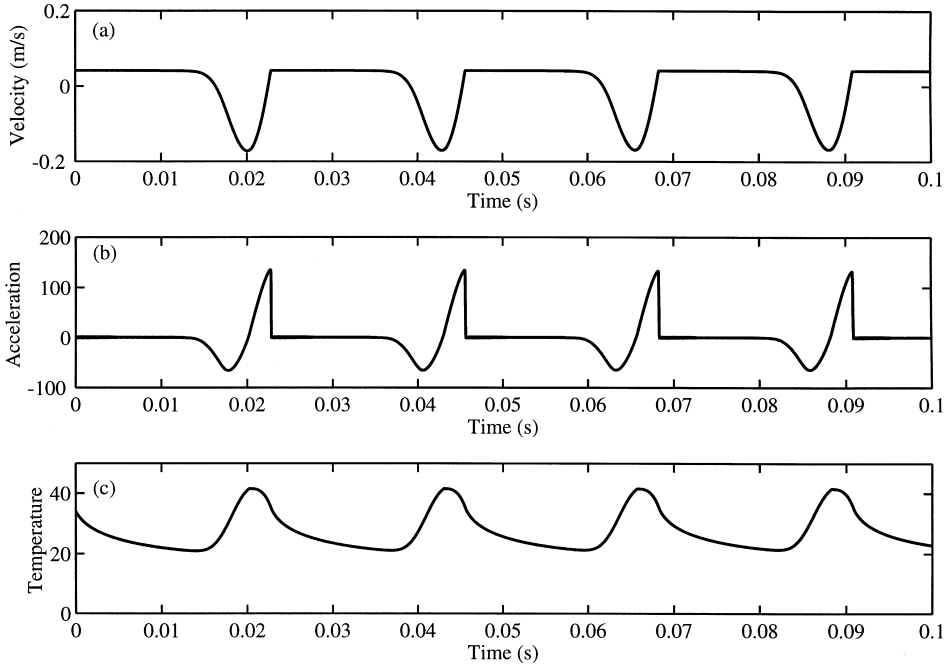

Fig. 24. Simulation of stick–slip motion using the oscillator model and the plastic-yield frictional law depending on contact temperature. Rod speed and normal force were as for Fig. 6. Velocity (a), acceleration (b) and temperature (c) plotted on the same horizontal and vertical scales as Fig. 6.

temperature/velocity curve shows a clockwise hysteresis loop, showing again how the frictional hysteresis has its origin in thermal inertia.

Based on this single case, the plastic-yield constitutive model performs rather well in comparison with the experiments. To test this more thoroughly, we explore the effect of changing parameters. The simulation program has been run for the set of six cases chosen to illustrate the experimental behaviour. The layer thickness was kept unchanged throughout, while the contact radius was varied in proportion to the square root of the normal load, as explained previously. First, we show the variation of acceleration waveform as the rod speed is varied. Fig. 26 shows results which are directly comparable with Fig. 8. The comparison is very satisfactory. The frequency of stick–slip vibration varies in very much the same way as was observed, and the amplitude and shape details of the waveforms are very close.

In Fig. 27 the friction/velocity curves for all six cases are overlaid on the measurements (reproduced from Fig. 9). The comparison with measurements is by no means perfect, but some trends are reproduced fairly well. Except perhaps for cases c and d the agreement is clearly closer than that shown in Fig. 23(a). All cases show hysteresis in the correct sense. The loops tend to be more open with lower rod speed, turning to long and thin forms at high rod speed. The peak sliding speed is roughly correct (except in case d). Indeed, it should be noted that the peak sliding speed in the measurements often varied from cycle to cycle by amounts comparable with the discrepancies seen here between theory and experiment.

To discuss detailed discrepancies it is useful to see also the temperature variation, shown in Fig. 28 in the form of temperature/velocity curves. It is immediately clear that the four cases which gave quite good agreement in Fig. 27(a), (b), (e) and (f) all have temperature fluctuations in roughly the same range, while the two cases which did not agree (c, d) had significantly different

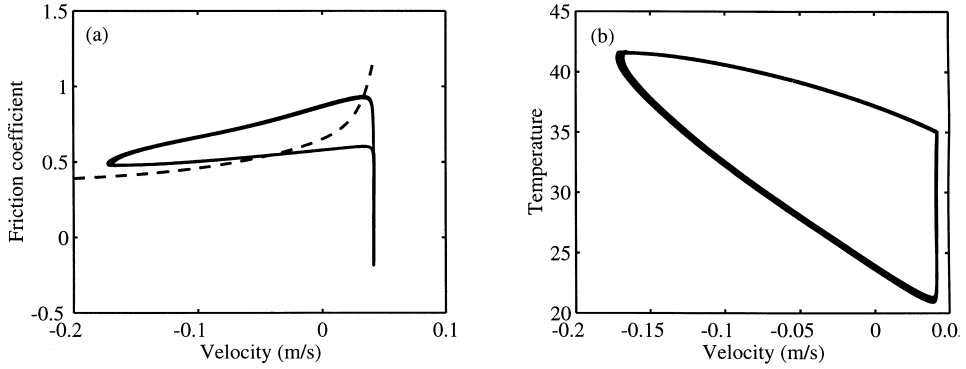

Fig. 25. Coefficient of friction versus oscillator velocity (a) and contact temperature versus sliding velocity (b), for the simulated stick–slip motion shown in Fig. 24. The friction/velocity characteristic from steady sliding measurements is shown in (a) as a dashed line.

temperatures. This gives a clue as to the explanation. Fig. 27(c) showed a loop of the right shape, but the absolute value of the coefficient of friction was too low throughout. This fact arises directly from the fact that the temperature is rather high but perhaps in practice under these conditions the higher temperature would lead to growth of the contact area, which in turn might reduce the temperature. In the real system the contact zone is self-adjusting, but there is no mechanism for this within the present (very simple) model. Similarly, Fig. 27(d) shows a clear discrepancy in the maximum slipping speed, and hence in the appearance of the hysteresis loop. In this case the contact temperature is anomalously low, and perhaps the assumed contact radius is too large.

Of course it might be possible to use ad hoc parameter adjustments for each separate case to achieve the best match to measurements. However, little physical insight is gained by introducing further disposable parameters into the theory. The model was constructed to be the simplest idealisation which included the temperature effect, and it would not be reasonable to expect from it perfect agreement with experiments. On the whole, the extent of agreement revealed by Figs. 27 and 28 is very encouraging, and suggests that this model captures something of the true physical description of rosin tribology. To go beyond this

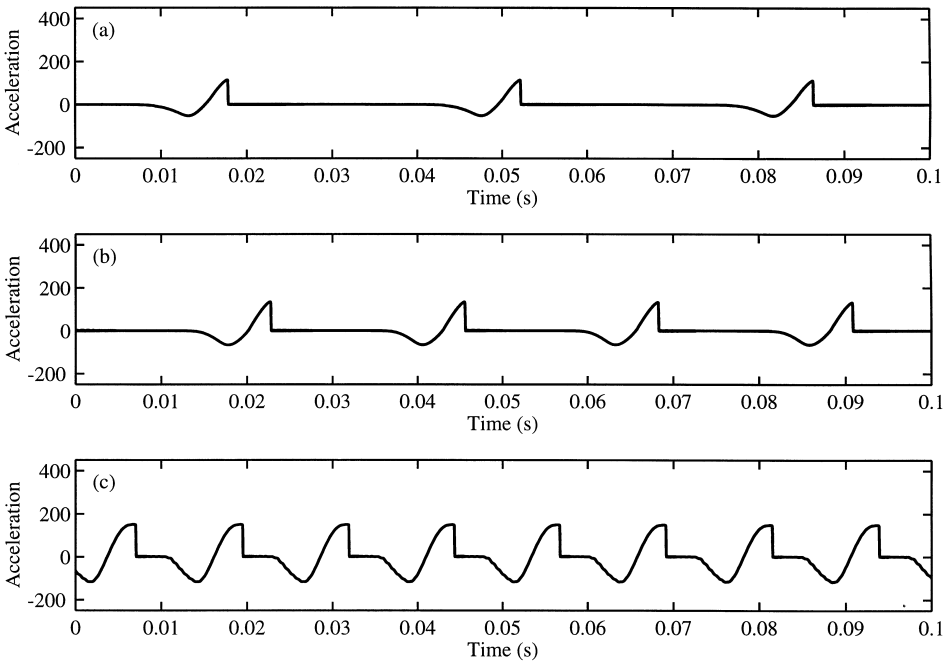

Fig. 26. Acceleration waveforms simulated using the plastic-yield frictional law with normal force 6 N: (a) rod speed 0.024 m/s; (b) rod speed 0.042 m/s (as in Fig. 24); (c) rod speed 0.13 m/s. These results are directly comparable with Fig. 8.

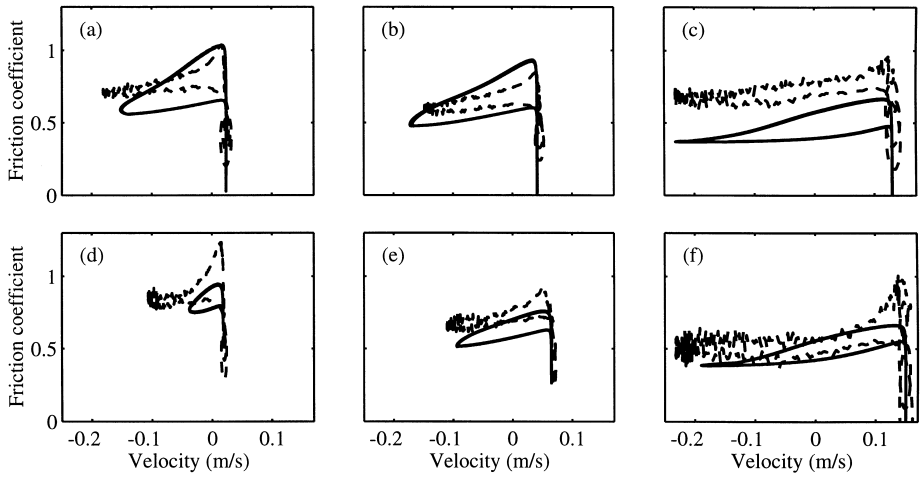

Fig. 27. Friction/velocity characteristics simulated using the plastic-yield frictional law (solid lines) and measured (dashed lines): (a) rod speed 0.024 m/s, normal force 6 N; (b) rod speed 0.042 m/s, normal force 6 N; (c) rod speed 0.13 m/s, normal force 6 N (d) rod speed 0.019 m/s, normal force 3 N; (e) rod speed 0.065 m/s, normal force 3 N; (f) rod speed 0.15 m/s, normal force 3 N. The measurements are reproduced from Fig. 9.

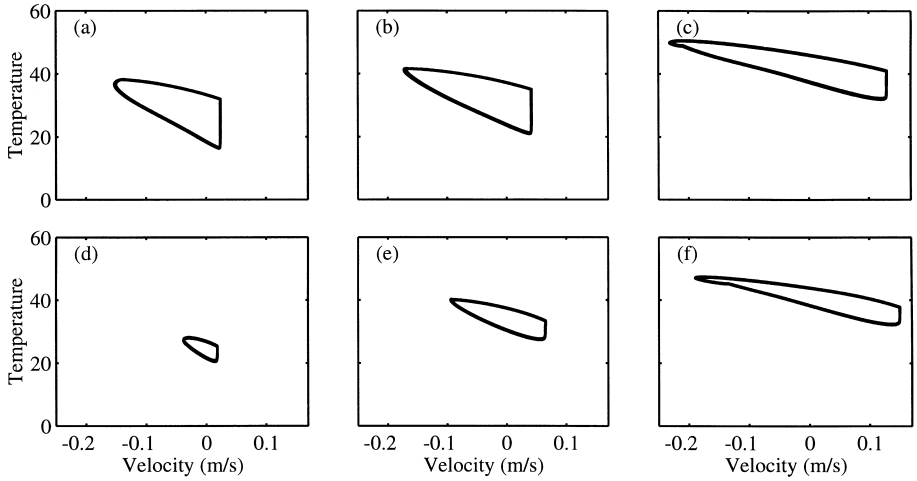

Fig. 28. Contact temperature (above ambient) versus velocity for the six simulations shown in Fig. 27.

one should surely include more physics in the model, rather than introduce "twiddle factors".

7. Conclusions

The experimental apparatus described in this paper provides a reasonably reliable method for the measurement of steady sliding and stick–slip friction characteristics for a film of rosin deposited on a range of substrate materials. Tests have been made over a wide range of sliding speeds and normal forces. In all cases, hysteresis was observed in the measured friction/velocity characteristics. For the stick–slip results, no portion of the hysteresis loops followed the friction/velocity relation found from steady-sliding tests. This provides clear evidence that state variables other than the instantaneous sliding velocity play a significant role in the frictional behaviour of rosin.

Two models for the tribology of rosin coated surfaces have been discussed. Both are based on thermal modelling somewhat similar to that used by Evans et al. (1975) to model the friction behaviour of ice, in which a consideration of the heat flow at the sliding contact enables the bulk temperature and hence the friction coefficient to be calculated. In this case, however, physical mechanisms for the friction force have been proposed, arising from either viscous shear or plastic yielding of a layer of rosin. This thermal modelling was motivated by direct evidence, reported here, that partial melting of rosin occurs under frictional conditions similar to those used in stick–slip experiments.

The models explain the falling friction–velocity characteristic, measured during steady sliding experiments, in terms of melt lubrication. As the sliding velocity increases, the temperature of the rosin layer rises and its viscosity and/or shear yield strength drops, in either case resulting in a reduced resistance to sliding. This description gives a physical interpretation for the hysteresis observed in the measured stick–slip friction–velocity characteristics of rosin coated surfaces. Hysteresis arises because thermal inertia causes a time lag, the temperature of the rosin layer takes a finite time to respond to the changes in sliding speed.

The predictions of both models have been compared with experiments using forced sinusoidal sliding and self-excited stick–slip vibration. The results for sinusoidal sliding were encouraging, with the viscous model perhaps matching the experiments more closely than the plastic-yield model. For the case of stick–slip motion the viscous model did not give satisfactory predictions. Simulations based on the plastic-yield model, however, gave very encouraging agreement with the measurements. Stick–slip vibrations were predicted with periods and amplitudes of vibration in the correct region, and with details of waveforms (including the hysteresis loops) quite closely matching those seen in practice. This model certainly gives a better quantitative description of stick–slip behaviour than a model in which the instantaneous sliding speed is the only state variable. It seems very plausible that the true physical explanation of rosin tribology under the conditions of these experiments is along the lines of this plastic-yield model.

The very simple model presented here does not attempt to describe all the details of the behaviour. The thermal model was deliberately formulated in terms of a single, averaged temperature in the contact region, and the heat flow into the substrate materials was modelled by one-dimensional diffusion. The main shortcoming of this model is that it gives no systematic way to assess the effect of genuinely three-dimensional effects, such as the variation of temperature and material properties through the contact region. It also gives no basis for a convincing determination of the size and thickness of the softened layer of rosin in the contact region, and other arguments had to be used to estimate these geometric parameters. To go beyond this approximation would need considerably more elaborate modelling, and correspondingly more elaborate experiments.

A target for further research will be to apply this model to the simulation of bowed-string motion. Such simulations have been carried out quite extensively in the past (McIntyre and Woodhouse, 1979; McIntyre et al., 1983; Schumacher and Woodhouse, 1995; Pitteroff and Woodhouse, 1998), but always using a friction law in which force depends only on relative sliding speed. It is likely that this new model will predict behaviour which is different in detail, and perhaps amenable to direct experimental test. An immediate target will be to resolve an apparent paradox. Within the framework of a simple friction–velocity law, a kind of hysteresis occurs when normal force exceeds a threshold value (McIntyre and Woodhouse, 1979), and this causes the vibration frequency to fall. This "flattening effect" is commonly observed in violin playing and does indeed seem to require normal force to exceed a threshold value (Faure and Boutillon, 1993; Schumacher, 1994). The model developed here appears to predict the occurrence of a hysteresis loop at *all* levels of normal force, and thus will perhaps predict no threshold for the flattening effect. A careful study will be needed to see if the model predictions indeed conflict with observations.

Acknowledgements

The authors wish to thank Professors K.L. Johnson, M.F. Ashby and R.S. Langley for their invaluable advice in developing the theoretical model, Dr. C.Y. Barlow and Mr A. Heaver for expert assistance with the scanning electron microscope, and Dr. M.R. Mackley and Mr. R. Marshall for the rheometer measurements.

References

Askenfelt, A., 1989. Measurements of the bowing parameters in violin playing. Part II: Bow-bridge distance, dynamic range and limits of bow force. J. Acoust. Soc. Amer. 86, 503–516.

Bowden, F.P., Hughes, T.P., 1939. The mechanism of sliding on ice and snow. Proc. Royal Soc. London A172, 290–298.

Carslaw, H.S., Jaeger, J.C., 1959. Conduction of Heat in Solids. Clarendon Press, Oxford.

Cobbold, P.R., Jackson, M.P.A., 1992. Gum rosin (colophony): a suitable material for thermomechanical modelling of the lithosphere. Tectonophysics 210, 255–271.
Evans, D.C.B., Nye, J.F., Cheeseman, K.J., 1975. The kinetic friction of ice. Proc. Royal Soc. London A347, 493–512.
Faure, C.-A., Boutillon, X., 1993. Détermination et étude expérimentale de la fréquence d'oscillation d'une corde frotté. Comptes Rendus de l'Académie des Sciences de Paris 317, 1377–1382.
Johnson, K.L., 1985. Contact Mechanics. Cambridge University Press, Cambridge.
Kaye, G.W.C., Laby, T.H., 1986. Tables of Physical and Chemical Constants, 15th ed. Longman, New York.
Ko, P.L., Brockley, C.A., 1970. The measurement of friction and friction-induced vibration. Trans. ASME: Journal of Lubrication Technology 92, 543–549.
Lazarus H., 1972. Die Behandlung der selbsterregten Kippschwingungen der gestrichenen Saite mit Hilfe der endlichen Laplacetransformation. Dissertation, Technical University of Berlin.
Lighthill, M.J., 1958. An Introduction to Fourier Analysis and Generalised Functions. Cambridge University Press, Cambridge.
Lim, S.C., Ashby, M.F., 1987. Wear-mechanism maps. Acta Metallurgica 35, 1–24.
McIntyre, M.E., Woodhouse, J., 1979. Fundamentals of bowed-string dynamics. Acustica 43, 93–108.
McIntyre, M.E., Schumacher, R.T., Woodhouse, J., 1983. On the oscillations of musical instruments. J. Acoust. Soc. Amer. 74, 1325–1345.
Pickering, N.C., 1992. The Bowed String. Amereon, Mattituck, New York.
Pitteroff, R., Woodhouse, J., 1998. Mechanics of the contact area between a violin bow and a string. Part II: Simulating the bowed string. Acustica Acta Acustica 84, 744–757.
Ruina, A., 1983. Slip instability and state variable friction laws. J. Geophys. Res. 8, 10359–10370.
Schumacher, R.T., 1994. Measurements of some parameters of bowing. J. Acoust. Soc. Amer. 96, 1985–1998.
Schumacher, R.T., 1997. Measurement of bow force. Proc. Inst. Acoustics 19 (5), 43–48 (See figure 2).
Schumacher, R.T., Woodhouse, J., 1995. The transient behaviour of models of bowed-string motion. Chaos 5, 509–523.
Skudrzyk, E., 1968. Simple and Complex Vibratory Systems. Pennsylvania State University Press, Pennsylvania.
Sternlicht, B., Apkarian, H., 1960. Investigation of melt lubrication. Trans. ASLE 2, 248–256.
Tabor, D., 1979. Gases, Liquids and Solids. Cambridge University Press, Cambridge.
Tolstoi, D.M., 1967. Significance of the normal degree of freedom and natural normal vibrations in contact friction. Wear 10, 199–213.
Woodhouse, J., 1993. On the playability of violins. Part I: Reflection functions. Acustica 78, 125–136.